

NASA CONTRACTOR REPORT 177538

1N-31  
1642  
P84

## INTEGRATED CRYOGENIC EXPERIMENT (ICE) MICROSPHERE INVESTIGATION

I. Spradley

D. Read

NASA  
Contract NAS2-12897  
September 1989

(NASA-CR-177538) INTEGRATED CRYOGENIC  
EXPERIMENT (ICE) MICROSPHERE INVESTIGATION  
(Lockheed Missiles and Space Co.) 84 p

CSCL 13B

G3/31

N91-19323

Unclas  
0001642

**NASA CONTRACTOR REPORT 177538**

**INTEGRATED CRYOGENIC EXPERIMENT (ICE) MICROSPHERE INVESTIGATION**

**I. Spradley**

**D. Read**

**Lockheed Missiles & Space Company, Inc.  
Research & Development Division  
Palo Alto, California 94304**

**Prepared for  
NASA  
Ames Research Center  
Under Contract NAS2-12897  
September 1989**

## FOREWORD

This work was conducted for the National Aeronautics and Space Administration (NASA) through the Ames Research Center, Moffett Field, California, Jeff M. Lee, Program Manager.

The Research & Development Division of Lockheed Missiles & Space Company, Inc. (LMSC), conducted the program in the Cryogenic Technology Group of the Thermal Sciences Laboratory. Key individuals who contributed to this program are:

- A. Collaco – Designed microsphere test cells
- D. Robertson – Designed control and interface electronics
- C. Kirk – Assembled microsphere test cell

Principal Investigators:

I. Spradley

D. Read

## CONTENTS

Section		Page
1	INTRODUCTION	1-1
	1.1 Overview	1-1
	1.2 Proposed Experiment Objectives	1-4
2	MICROSPHERE CHARACTERISTICS AND ANALYSIS OF MICROSPHERE THERMAL PERFORMANCE	2-1
3	EXPERIMENT DESIGN	3-1
	3.1 Conceptual Design	3-1
	3.2 Preliminary Experiment Design Concept	3-1
	3.3 Experiment Design	3-2
	3.3.1 Design Concept	3-2
	3.3.2 Performance Characteristics	3-7
	3.4 Ground Test	3-11
	3.4.1 Ground Test Design	3-11
	3.4.2 Test Article Fabrication and Assembly	3-13
	3.4.3 Test Setup	3-21
	3.4.4 Test Results and Conclusions	3-24
	3.5 Flight Experiment Package	3-30
	3.5.1 Microsphere Flight Experiment	3-30
	3.5.2 Microsphere Test Internal Electronics	3-32
	3.5.3 Low-g Performance of PODS	3-32
	3.6 Integration of Flight Experiment with HELD	3-32
	3.6.1 Integration With HELD	3-32
	3.6.2 Integration with IFPA	3-33
	3.6.3 Lifetime	3-36
	3.6.4 Ground Hold	3-36
4	INTEGRATION WITH HOST SPACECRAFT	4-1
	4.1 Hitchhiker M	4-1
	4.1.1 Mechanical Interface	4-1
	4.1.2 Plumbing Interface	4-1
	4.1.3 Electrical/Data Interface	4-5
	4.1.4 Customer Ground Support Equipment	4-6
	4.1.5 Measurement Electronics Payload	4-7
	4.2 Safety	4-8
	4.2.1 HELD Dewar Structural Analysis	4-8
	4.2.2 HELD Catastrophic Vent Analysis	4-9

<b>Section</b>	<b>Page</b>
5      APPLICATIONS	5-1
6      PRELIMINARY COST ESTIMATE	6-1
7      SUMMARY AND CONCLUSIONS	7-1
8      REFERENCES	8-1

## ILLUSTRATIONS

Figure		Page
1-1	HELD	1-3
2-1	Comparison of Calculated and Measured Heat Rates	2-3
2-2	Effect of Gravity on Microsphere Performance	2-4
2-3	Comparison of Microsphere and MLI Performance	2-5
2-4	Effect of Insulation Thickness on Microsphere Performance	2-6
2-5	Effect of Boundary Emissivity on Insulation Performance Predictions	2-7
2-6	Comparison of Uncoated and Metallized Microsphere Performance Predictions in Low-g	2-8
2-7	Effect of Conduction on Uncoated-Microsphere Performance	2-9
2-8	Effect of Conduction on Metallized-Microsphere Performance	2-10
2-9	Effect of Conduction on Microsphere Performance	2-10
2-10	Comparison of Microsphere and MLI Performance Predictions	2-11
3-1	Preliminary Design Concept	3-2
3-2	Preliminary Concept Heat Map for Uncoated Microspheres in 0 g	3-3
3-3	Insulation Experiment Cell	3-4
3-4	Isothermal Cavity Heat Map for Uncoated Microspheres in 0 g	3-5
3-5	Effect of Hot-Boundary Tube Diameter on Microsphere Resistance	3-6
3-6	Effect of Insulation Test Section Length on Microsphere Resistance	3-6
3-7	Effect of Insulation Test Section Thickness on Microsphere Resistance	3-7
3-8	Comparison of Insulation Performance Predictions	3-8
3-9	Transient Response of Metallized Microspheres	3-9
3-10	Transient Response of Uncoated Microspheres	3-10
3-11	Power Required to Warm Microsphere Test Setup	3-11
3-12	Proposed Microsphere Test Sequence Transient Response for Metallized Microspheres	3-12
3-13	Proposed Microsphere Test Sequence Transient Response for Uncoated Microspheres	3-13
3-14	Sensitivity of Heat Rate Measurements to Isothermal Cavity Temperature Differentials, Metallized Microspheres in 0 g	3-14
3-15	Sensitivity of Heat Rate Measurements to Isothermal Cavity Temperature Differentials, Uncoated Microspheres in 0 g	3-15

<b>Figure</b>		<b>Page</b>
3-16	Sensitivity of Heat Rate Measurements to Isothermal Cavity Temperature Differentials, Uncoated Microspheres in 1 g	3-16
3-17	Test Article Component	3-16
3-18	Test Article Vacuum Enclosure	3-17
3-19	Test Article Internal Components	3-18
3-20	Hot-Temperature Boundary Tube	3-19
3-21	Central Temperature Control Tube and End Disks	3-20
3-22	Central Tube Support Tube	3-20
3-23	Hot-Boundary Support Tube	3-20
3-24	20-mm Filter	3-21
3-25	Diode Placement	3-22
3-26	Central Tube Assembly	3-22
3-27	Instrumentation Wiring From End Cap	3-23
3-28	Central Tube Instrumentation Wiring	3-23
3-29	Internal Assembly and Wiring	3-24
3-30	Internal Assembly, End View	3-24
3-31	Complete Internal Assembly	3-25
3-32	Low-Emittance Hot-Boundary Surface	3-25
3-33	Assembly Filled With Microspheres	3-26
3-34	Completed Microsphere 1-g Test Assembly	3-27
3-35	Microsphere Test Setup During Pumpdown	3-28
3-36	Microsphere in Test Assembly Suspended in LN <sub>2</sub> Dewar	3-29
3-37	Uncoated-Microsphere Ground Test	3-30
3-38	Microsphere Flight Experiment	3-31
3-39	Power Requirements for Microsphere Heaters	3-33
3-40	Integration of Experiment Into HELD	3-34
3-41	HELD Design Layout	3-35
3-42	IFPA/Microsphere Assembly	3-37
3-43	Effect of Experiment Heat Rate on HELD Lifetime	3-37
4-1	HH-M	4-2
4-2	HELD-HHM Integration (Front View)	4-3
4-3	HELD-HHM Integration (Side View)	4-4
4-4	Fluid System	4-5
4-5	Ice Microsphere Payload System Configuration	4-6
4-6	Ice Microsphere Measurement System Block Diagram	4-7
4-7	HELD Plumbing Diagram	4-10
4-8	SFHe Tank Pressure After Burst of BD-1	4-14
4-9	SFHe Tank Pressure After Burst of BD-2	4-14
6-1	Microsphere WBS	6-2
6-2	Microsphere Program Schedule	6-3
6-3	Test Flow	6-4

## TABLES

<b>Table</b>		<b>Page</b>
2-1	Utilization by NASA Programs of Technologies Demonstrated by HELD	1-5
4-1	Weight Summary	4-4
5-1	Long-Term Cryogen Storage Applications for Microspheres	5-2

## Section 1

### INTRODUCTION

#### 1.1 OVERVIEW

The lifetime of a cryogenic system is highly dependent on the parasitic heat leak to the cryogen. The heat leak through the insulation system is often one of the largest components of the total parasitic heat leak; hence, it greatly affects system lifetime. Substantial benefits could be realized from improved insulation systems, since they are a major component in determining the lifetime and cost of cryogenic systems. Microsphere insulation has the potential to perform better than current multilayer insulation (MLI) under certain conditions. Microspheres are small (20 to 120  $\mu\text{m}$  in diameter) hollow glass spheres that can be coated with a low-emittance surface to reduce radiation heat transfer. When used in the insulation space, these packed spheres serve as a radiation shield to reduce the radiation heat transfer, providing conduction through the contacting spheres. The potential advantages of microspheres over MLI are:

- Better performance in a 0-g environment at low boundary temperatures
- Easier installation, resulting in reduced assembly costs
- Better performance with difficult wrap geometries
- Improved repeatability, since performance is not sensitive to wrapping techniques

The microsphere insulation investigation is one of 41 outreach proposals that have been funded for a definition study. The experiment will investigate cryogenic and long-term cryogenic storage in the fuel storage and transfer section of the fluid management theme. The goal of the outreach program is to identify key technology areas that require a space experiment for verification and validation. A space demonstration of microsphere insulation

is required, since predictions indicate that the performance should be greatly enhanced by a low-g environment. In low-g, radiation is the only heat transfer mechanism. Conduction through the spheres is essentially zero, since there is no contact force between the spheres. Because radiation transfer through packed spheres in a low-g environment is difficult to analyze, a space experiment to verify performance is required.

Previous work has demonstrated that the microsphere insulation system is viable for use in cryogenics (Ref. 1). Microspheres have been extensively tested on the ground between 300 K and liquid-nitrogen temperatures (Refs. 2, 3). The effects of microsphere size and coating (coated with low-emittance metal, partially-coated, and uncoated) have been investigated. The combination of these effects has also been tested. Analysis indicates that the overall performance of this type of insulation would be greatly enhanced by a low-g environment. To date, there are no ground-based tests that can provide the data required to confirm this belief. The low-g test times in a drop-tower, parabolic flight, or sounding rocket are too short for a meaningful thermal test. Consequently, an orbital test is required to demonstrate the low-g characteristics of this type of insulation.

A benefit of this program is that a superfluid helium (SFHe) dewar that could be used as a test bed and cold temperature sink for the experiment has been developed by Lockheed Missiles & Space Company, Inc. (LMSC). The Helium Extended Life Dewar (HELD) is an Independent Development project which has served as a demonstration of LMSC's SFHe capabilities. It is proposed that the microsphere experiment be integrated into the instrument tunnel of HELD. Some of the details of HELD are shown in Fig.1-1.

HELD provides a convenient design that allows easy access to experiments installed in its instrument well. The design would allow experiments that require SFHe cooling to be integrated together into a larger experiment package requiring only one flight. The purpose of HELD is to demonstrate long-term storage of SFHe in orbit for a variety of purposes. By using technological advances such as improved MLI and newly developed support struts [Passive Orbital Disconnect Struts (PODS)], a multiyear SFHe storage system has been developed.

The support system for the HELD is the PODS (Refs. 6, 7, 8, 9), an advanced low-conductance support system that has been extensively tested on the ground but not yet tested in space. Concern over possible dynamic coupling between the PODS and the sloshing liquid

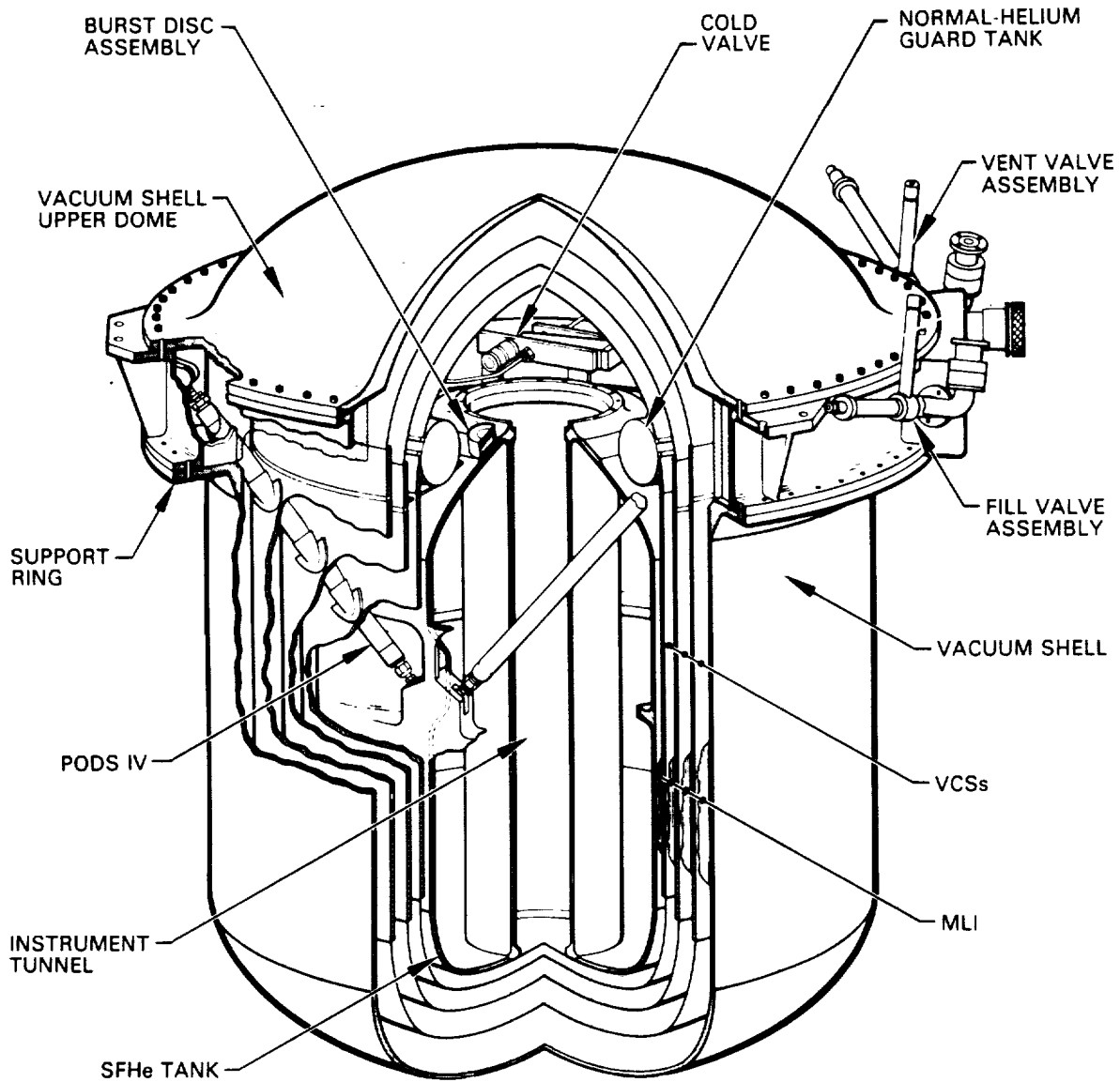


Fig. 1-1 HELD

helium (LHe) has suggested that a flight demonstration/investigation be conducted, since this coupling cannot be measured or fully investigated on the ground. Therefore, in addition to serving as a test bed for the microspheres, HELD will allow characterization of the dynamic properties of PODS in a low-g environment. Results of the characterization of PODS dynamic response in orbit can be applied to other liquid-cryogen cooling/storage

systems. HELD and PODS have been designed and built and are currently undergoing extensive thermal and structural testing.

Many NASA programs will benefit from the specific technologies that will be demonstrated by using HELD to support these experiments. These technologies include:

- PODS
- Cold valves
- Improved MLI
- Low-conductance fill line
- Porous-plug vent
- PODS-supported vapor-cooled shields
- Normal-helium guard tank for simplified prelaunch servicing
- Cold burst disk

The items listed above are critical to long-term cryogen storage, especially superfluid helium. Table 1-2 lists the NASA programs that would benefit from a flight demonstration of these technologies.

Programs 1 through 5 all utilize superfluid helium, and flight demonstration of HELD components would benefit all of these programs. Program 6, COLD-SAT, is a hydrogen experiment that would also benefit from the advanced low-conductance technology incorporated into the HELD system.

In addition to HELD, the cryogenic facilities at the LMSC Research & Development Division (R&DD) Palo Alto Research Laboratories are available as required for development of the experiment. These facilities include ground dewar systems, large vacuum pumping systems, appropriate clean benches for assembly, and data acquisition systems for timely and accurate monitoring of experiments during ground testing.

## **1.2 PROPOSED EXPERIMENT OBJECTIVES**

The purpose of this experiment is to demonstrate the low-g insulating characteristics of various mixtures of microspheres and to:

Table 1-2 UTILIZATION BY NASA PROGRAMS OF TECHNOLOGIES DEMONSTRATED  
BY HELD

Program	Pods	Cold Valves	Normal-Helium Guard Tank	Phase Separator	Advanced Insulation	Cold Burst Disk	Vapor-Cooled Shields	Fill Line
1. SIRTf	X	X	X	X	X	X	X	X
2. AXAF (XRS)	X	X	X	X	X	X	X	X
3. Gravity Probe-B	X	X	X	X	X	X	X	X
4. Astromag	X	X	X	X	X	X	X	X
5. Superfluid Helium Tanker	X	X	X	X	X	X	X	X
6. COLD-SAT	X		X		X		X	X

X90677\_OSTABLES

- Compare 1-g and 0-g microsphere performance
- Determine microsphere performance over an appropriate range of boundary temperatures
- Determine microsphere performance as a function of boundary surface emittance
- Compare microsphere performance to reference insulations

The use of SFHe temperatures significantly reduces the radiation component of microsphere heat transfer, thus giving much better indication of solid-conduction heat transfer. The best method for achieving these low temperatures is to use HELD for the thermal test bed of the microsphere experiment. Use of HELD as the test bed for any SFHe experiments would result in the following two objectives being met:

- Characterization of PODS low-g dynamic properties readily becomes available.
- A flight demonstration of this system is done at relatively small cost.

The characterization of PODS in-orbit dynamic response could easily be included during the integration portion of the experiment, since PODS are the main support structure of HELD's SFHe tank.

## Section 2

### MICROSPHERE CHARACTERISTICS AND ANALYSIS OF MICROSPHERE THERMAL PERFORMANCE

The major heat transfer mechanism in packed spheres under evacuated conditions consists of the surface radiation transfer across the voids and the constricted conduction through the contact surface of packed particles. For a medium with coupled conduction and radiation transport, it has been shown that the effective thermal conductivity  $k$ , defined in the Fourier law  $q = -k(T) \partial T / \partial X$ , can be well approximated under most conditions as the linear summation of the conduction and radiation contributions. The conduction term is the additive sum of the constriction and gas-phase conduction contributions. Therefore, the effective thermal conductivity of the microsphere insulation is the sum of the solid conduction, gas conduction, and radiation conductivities:  $k = k_{sc} + k_{gc} + k_r$ . Since the microsphere insulation will be used in a vacuum, there will be no gas conduction, and the effective conductivity reduces to:

$$k = k_{sc} + k_r \quad (1)$$

Reference 1 contains the details of the analysis of the different components, with the resulting expressions for solid conduction ( $k_{sc}$ ) and radiation ( $k_r$ ), as follows:

$$k_{sc} = (1.07 \times 10^{-5})(P + H)^{0.535} [3.13 \times 10^{-3} T_H (1 + \theta) - 2.61 \times 10^{-6} T_H^2 (1 - \theta^3) / (1 - \theta)] \quad (2)$$

$$k_r = \left[ \frac{n^2}{0.75\beta l + \frac{1}{n\epsilon_H} + \frac{1}{n\epsilon_C} - 1} \right] \alpha T_H^3 (1 + \theta)(1 + \theta^2) \quad (3)$$

where

$$H = \text{integrated microsphere self-weight} \\ [1.87h - 0.00525 h^2 + 6.37 \times 10^{-6} h, \text{ Pa } (h^3 < 120 \text{ cm})]$$

$h$	= maximum vertical height (cm)
$k$	= thermal conductivity (W/m K)
$\ell$	= insulation thickness (m)
$n$	= refractive index of microspheres (uncoated = 1.56, metalized = 1.0)
$P$	= external compressive load (Pa)
$T_H, T_C$	= absolute hot and cold boundary temperatures, respectively (K)
$\beta$	= extinction coefficient of microspheres (uncoated = 9450 m <sup>-1</sup> , metalized = 56000 m <sup>-1</sup> )
$\epsilon_H, \epsilon_C$	= boundary temperature total hemispherical emittance $\epsilon(T) = 0.0067 \times T^{0.345}$ (Ref. 7)
$\theta$	= $T_C/T_H$
$\sigma$	= Stefan Boltzmann constant, $5.6 \times 10^{-8}$ (W/m <sup>2</sup> K <sup>4</sup> )

The previous work on microsphere thermal analysis and testing was performed for temperatures between 80 and 300 K under 1-g conditions. Figure 2-1 presents some of the test data obtained (Ref. 1) and the comparison to predictions. The very good agreement between the data and the predictions is partly due to the semiempirical nature of the analytic expressions. That some of the constants used in Eq. (1) for  $k_{sc}$  and  $k_r$  were experimentally derived helped to improve the correlation between predictions and test results. Due to the empirical nature of these expressions, they are only valid for the specific type of microsphere insulation tested (i.e., material, size, packing density, surface coating, emissivity). However, these equations can be modified by determining new constants for the type of microspheres used. For this study, it was assumed that microspheres similar to those tested previously would be used, and Eq. (1) as defined would be valid. This equation was used to determine microsphere performance and to evaluate the dependence of performance upon such parameters as surface coating and emissivity between 2 and 300 K.

Figure 2-2 shows the results of using these expressions to predict the performance of 0.25 in. of uncoated microsphere insulation with a 2-K cold boundary. Predictions of heat flux versus hot boundary temperature are shown for microspheres in 1-g, microspheres in 0-g, MLI with a degradation factor of 1.6, and flat plate radiation. The degradation factor is the ratio of actual thermal performance to predicted flat plate performance based on the MLI conduction equation derived from work reported in Ref. 8. The value of 1.6 is typical of

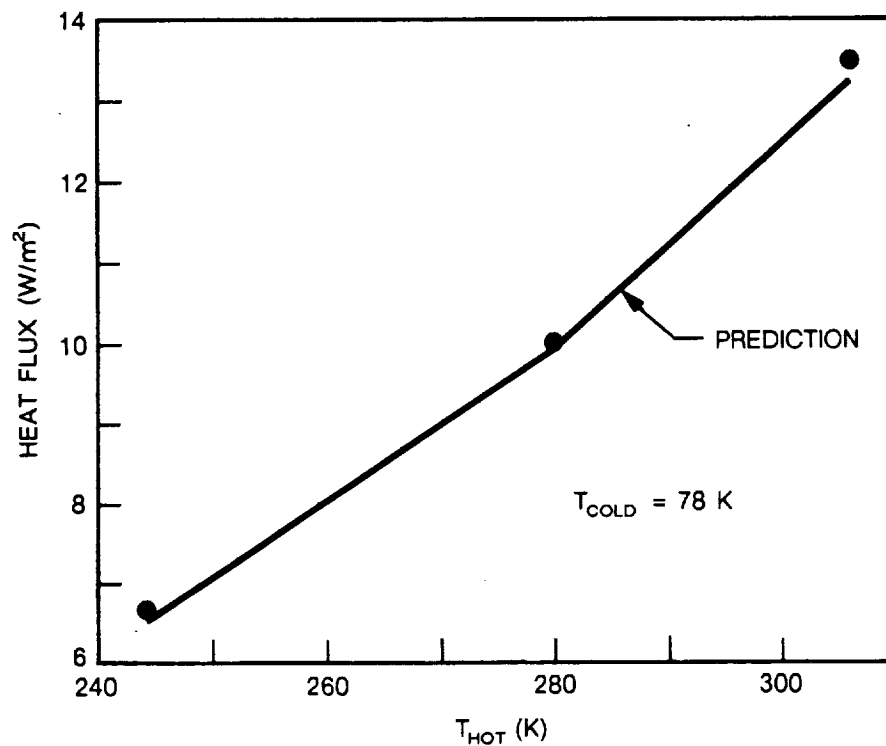


Fig. 2-1 Comparison of Calculated and Measured Heat Rates

the degradation factor encountered in flight cryogenic systems. Due to their isotropic nature, microspheres should not experience any degradation from flat-plate performance. Comparison of microspheres to MLI with a degradation factor of 1.6 should be representative of the performance of flight cryogenic systems. The performance of microspheres is greatly enhanced by the absence of gravity. This is because the conduction term in the effective conductivity is zero ( $k_{sc} = 0$ ), since there would be very little contact between the spheres in a low-g environment. Radiation is the only heat transfer mechanism in the 0-g prediction ( $k = k_r$ ), so the heat flux is decreasing with  $T_{HOT}$  to the fourth power.

The 1-g case contains the solid-conduction term, which is the dominant heat transfer mechanism at low temperatures, where the radiation transfer has been eliminated. Verification of the improved performance in 0-g is one reason that an orbital experiment is required. The prediction shows a factor of 2 reduction in heat flux at room temperature between the 1-g and 0-g conditions, and this difference increases with lower temperature.

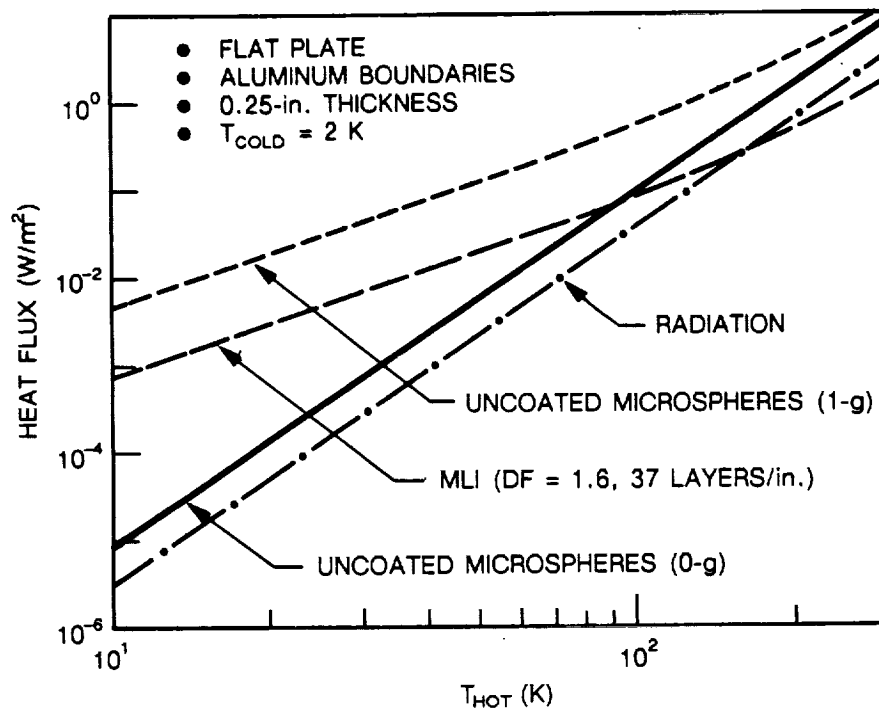


Fig. 2-2 Effect of Gravity on Microsphere Performance

The third curve is a prediction for MLI consisting of double aluminized mylar with a single silk net spacer. At room temperature, the heat flux through the MLI is lower than through the 1-g or 0-g microsphere insulation and is a factor of 4 lower than the 1-g microsphere prediction. The MLI and 1-g microsphere heat fluxes decrease at nearly the same rate, since the solid conduction dominates both insulations at the lower temperatures. The 0-g microsphere performance becomes better than MLI for hot boundary temperatures less than 150 K. This indicates that there is the potential for the microspheres to perform better than MLI for low boundary temperatures. The radiation performance indicates that at low temperatures ( $\leq 150$  K), low-emissivity boundaries with no insulation would be better than any of the insulations. This result is due to the extremely low emittance of the cold boundary at 2 K and the geometry used for the prediction. The assumed thickness was 0.25 in., which was based on the insulation thickness proposed for the experiment.

Figure 2-3 shows the same insulation systems as above, but this time, the heat flux is shown versus a variable cold boundary temperature and a constant hot boundary

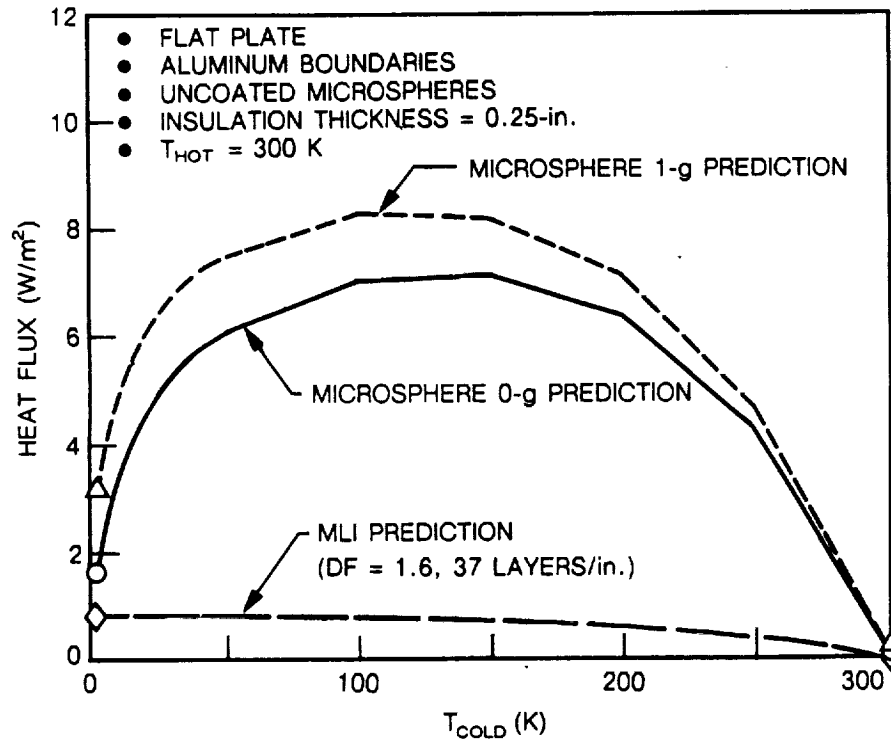


Fig. 2-3 Comparison of Microsphere and MLI Performance

temperature of 300 K. The results are very different from those of Fig. 2-2. There is still the improvement between the 1-g and 0-g cases, but it is a small difference at the high cold boundary temperatures. This is because the radiation transfer is 90% of the total above 250 K, so eliminating the conduction term in the 0-g case has little effect on the overall heat flux. The microsphere heat flux is higher than MLI. It first increases and then decreases with increasing cold boundary temperature. This behavior is due to the emissivity of the cold boundary surface which follows the following relationship for aluminum based on data from Ref. 7:  $\epsilon = 0.0067 \times T^{0.345}$ .

The emissivity of the cold boundary increases with temperature, and this increases the radiation transfer, even though the temperature differential decreases. The radiation heat transfer is a very weak function of the temperature difference and is driven by the hot boundary temperature and emissivity. This indicates that the microsphere performance is very dependent on the boundary emissivities, and that the use of microspheres may be limited to particular temperature regimes if minimum heat flux is required. The optimum use of microspheres may be in a hybrid insulation system, where MLI is used at the hot

boundary, with a transition to microspheres when the insulation temperature falls below the crossover temperature (100 to 150 K). This type of system would be ideal for vapor-cooled shield systems, where utilizing the shields to intercept heat flux through the insulation provides a convenient enclosure to contain the microspheres during assembly.

The effect of insulation thickness on heat flux is shown in Fig. 2-4 for uncoated microspheres in 0-g, MLI, and radiation. The radiation transfer is independent of the distance between the two surfaces, while the heat transfer through the microspheres and MLI decreases as the insulation thickness increases. The proposed experiment baseline of 0.25 in. between the hot and cold surfaces is at a thickness where having no insulating material would result in the best performance. The 0.25-in. thickness was not selected to give the optimum performance, but rather to increase the simplicity and accuracy of the experiment. This is the minimum thickness needed to get a reliable measure of performance while keeping the thermal resistance low, so that the time to reach steady-state operation can be kept to a minimum. A thicker insulation space would have better

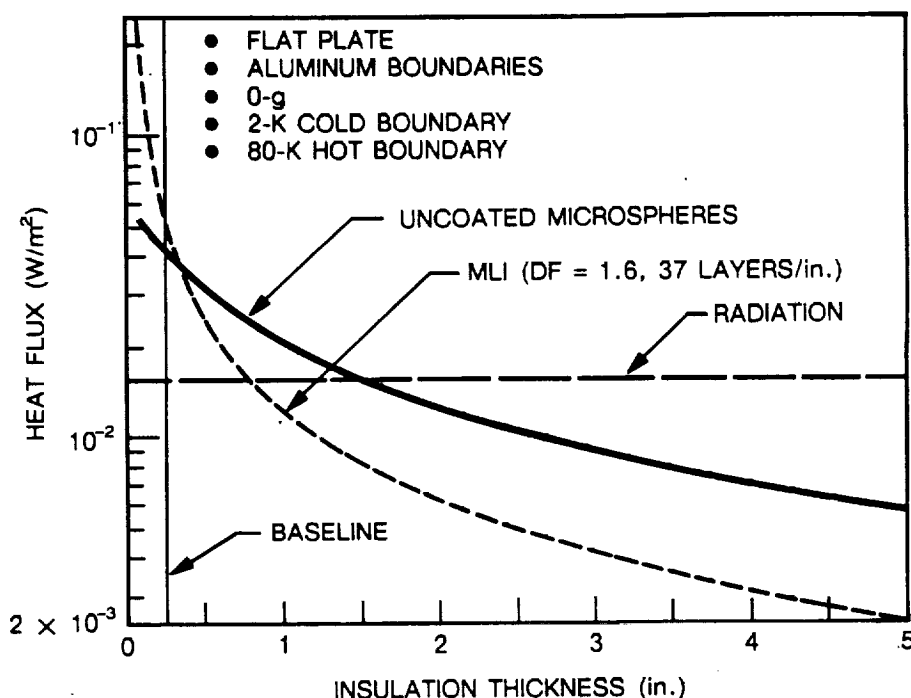


Fig. 2-4 Effect of Insulation Thickness on Microsphere Performance

performance, but it would decrease the accuracy of the performance measurement and not give any additional information concerning microsphere performance.

The effect of boundary emittance on microsphere thermal performance in 0-g was studied by examining at the impact of black boundaries on heat flux versus the low-emittance boundaries proposed for the experiment. The results are shown in Fig. 2-5. Black surfaces were examined for two reasons. A high-emissivity boundary may be of interest for the experiment, since this would increase the heat transfer and might simplify measurement requirements and improve accuracy. The black surface also serves to bound the effect of boundary emissivity by showing the maximum effect of boundary emissivity on performance. As shown in Fig. 2-5, the black surfaces increase the microsphere heat transfer by

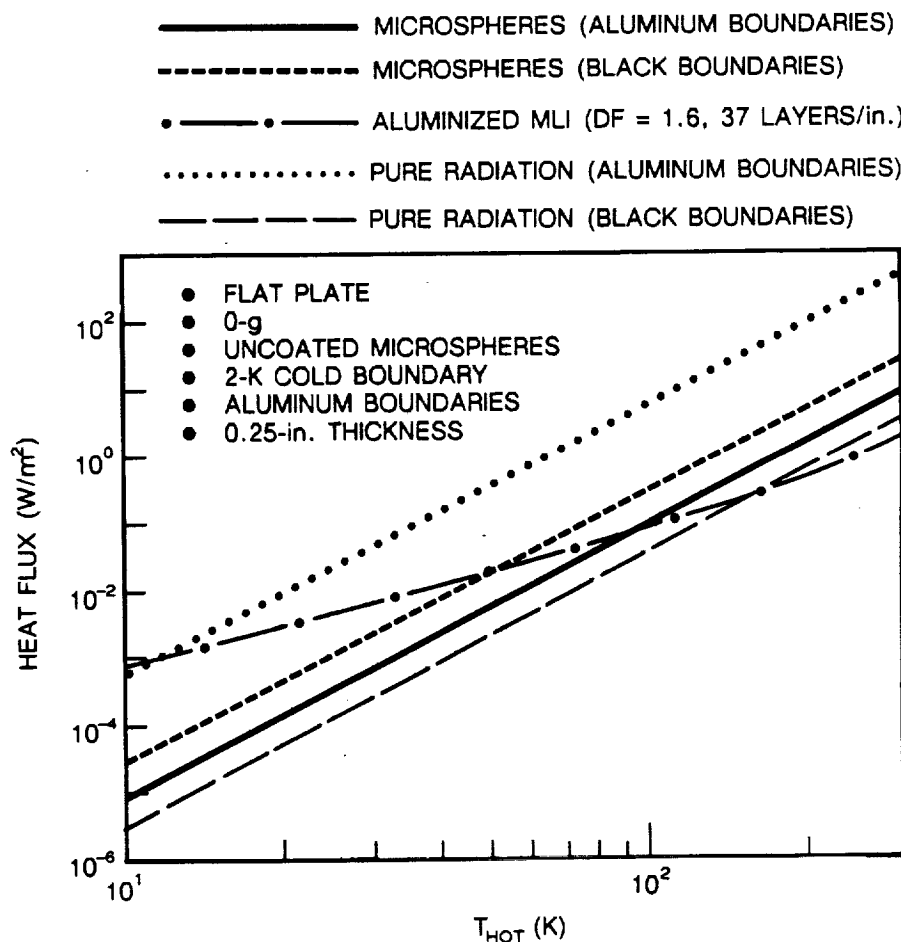


Fig. 2-5 Effect of Boundary Emissivity on Insulation Performance Prediction

a factor of 3. For radiation, the heat transfer is increased by 200 when black boundaries are introduced.

All of the microsphere thermal performance presented to this point has been for uncoated glass microspheres. Coating the spheres with a low-emissivity metal would improve their radiation performance by making the spheres a better radiation shield. This improves the performance in 0-g, where radiation is the only heat transfer mechanism. Figure 2-6 compares uncoated and metallized microspheres with MLI and radiation in a 0-g environment. Metallizing the microspheres lowers the heat flux by a factor of 8. The metallized microspheres perform better than MLI over the entire temperature range studied, while the uncoated microspheres are only better for hot boundary temperatures below 85 K.

The potential disadvantage to metallizing the microspheres is that the conduction heat transfer increases due to the lower contact resistance between the spheres. At high boundary temperatures, the metallized spheres would be better, since they are a better radiation shield, and radiation is the dominant heat transfer mechanism at high tempera-

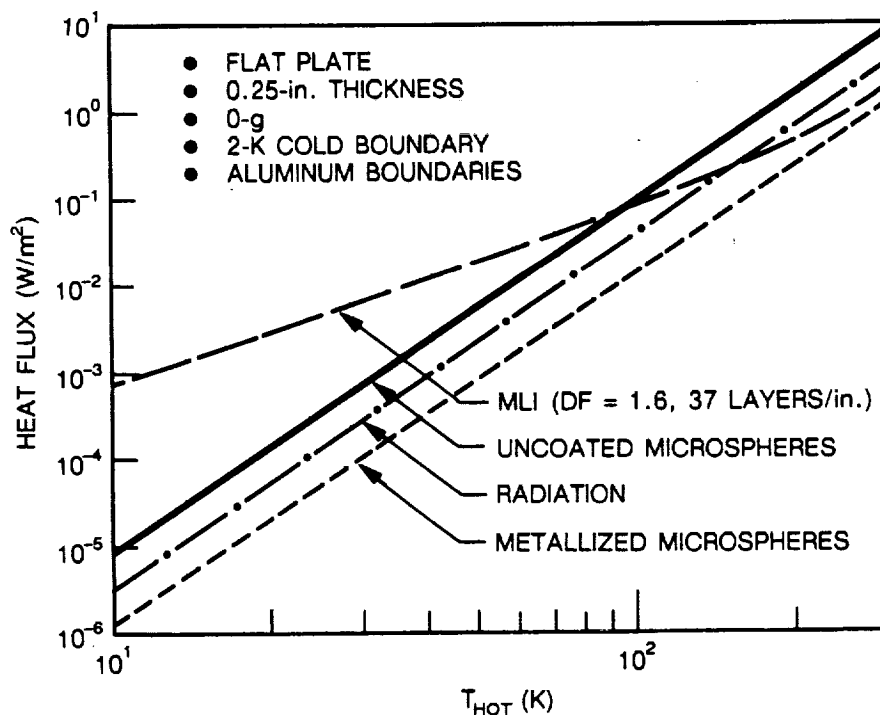


Fig. 2-6 Comparison of Uncoated and Metallized Microsphere Performance Predictions in Low-g

ture. At low temperatures, where conduction dominates, the uncoated spheres would be better, since the radiation component of the total heat flux is small and the performance of the microspheres as a radiation shield becomes less important. Figure 2-7 shows the performance of uncoated microspheres for a range of conduction percents. The 0% conduction corresponds to a 0-g environment, while the 100% conduction case is a 1-g environment. Near room temperature, the heat flux is essentially independent of conduction, because the heat transfer is dominated by radiation. At 70 K, the heat flux is reduced by a factor of 10 by eliminating conduction. Figure 2-8 shows the performance results for the metallized microspheres. Although the 0-g result is lower than for uncoated microspheres, the introduction of any conduction quickly increases the heat flux. The conduction is so much larger than the radiation conductance, even a small percentage of the conduction will dominate the heat transfer. Even at room temperature, the conduction component is still much larger than the radiation. Figure 2-9 summarizes the impact of conduction on microsphere performance. While the metallized spheres have the potential for the best performance, they are also the most sensitive to any increase in conduction

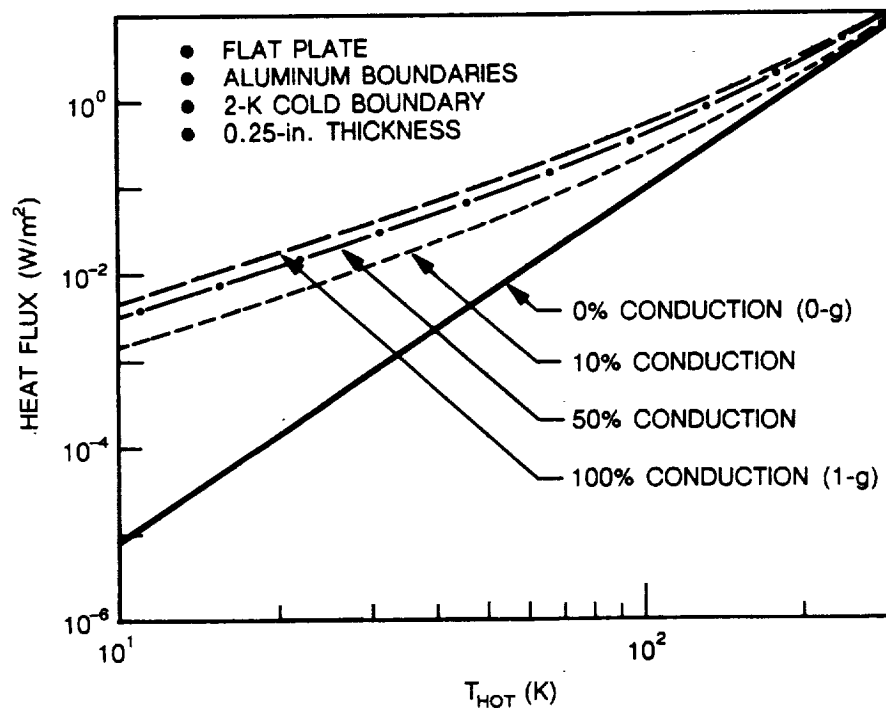


Fig. 2-7 Effect of Conduction on Uncoated-Microsphere Performance

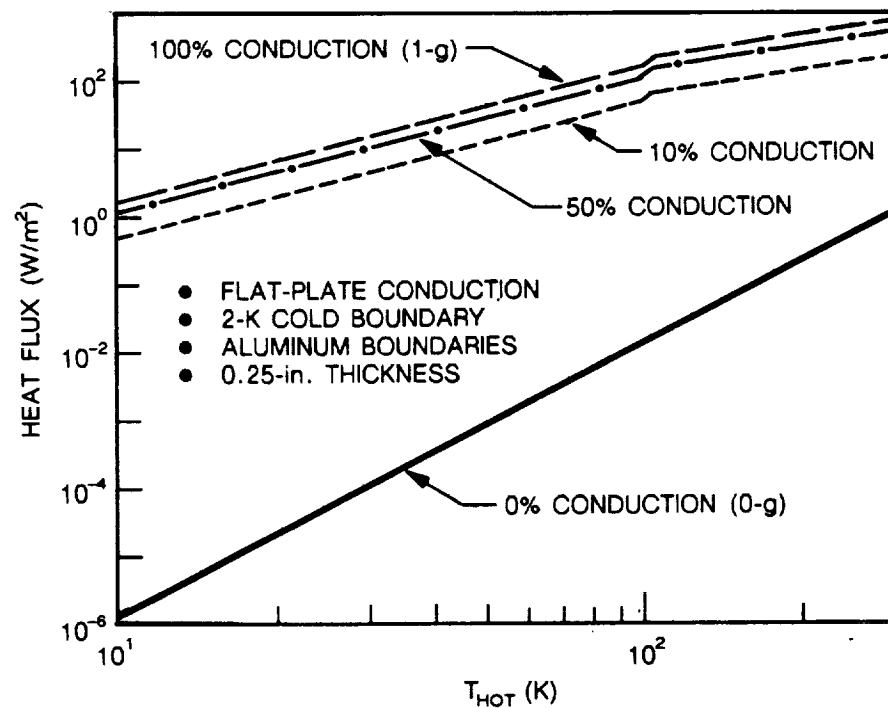


Fig. 2-8 Effect of Conduction on Metallized-Microsphere Performance

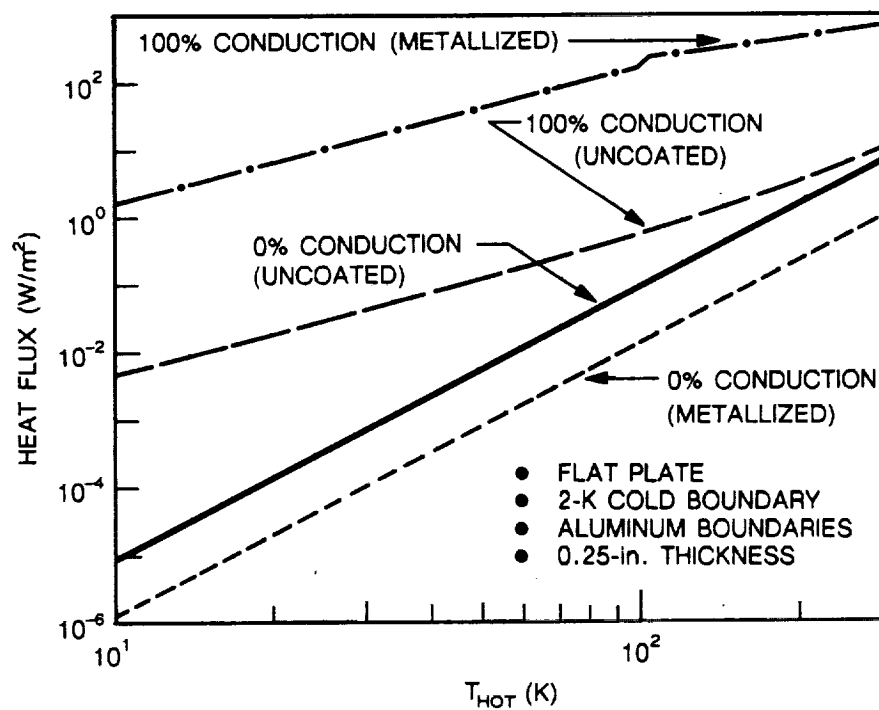


Fig. 2-9 Effect of Conduction on Microsphere Performance

due to contact between the spheres. The uncoated microspheres are less sensitive to increased conduction caused by contact between the spheres.

Figure 2-10 shows the range of expected flat-plate heat fluxes for the experiment during orbital operation. The range of expected results during ground testing would be represented by the 100% conduction curves for the metalized and uncoated microspheres.

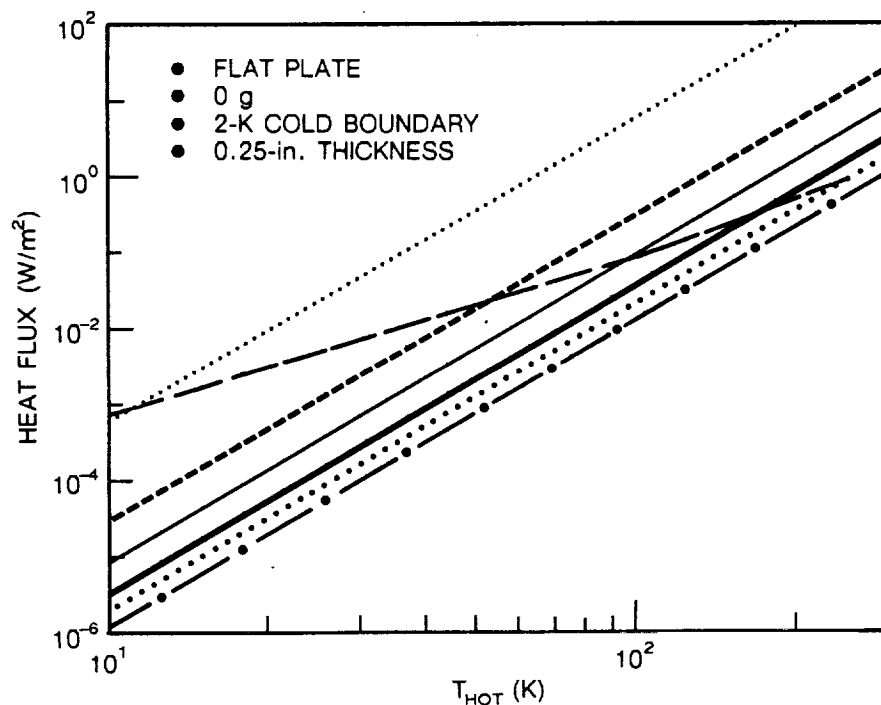
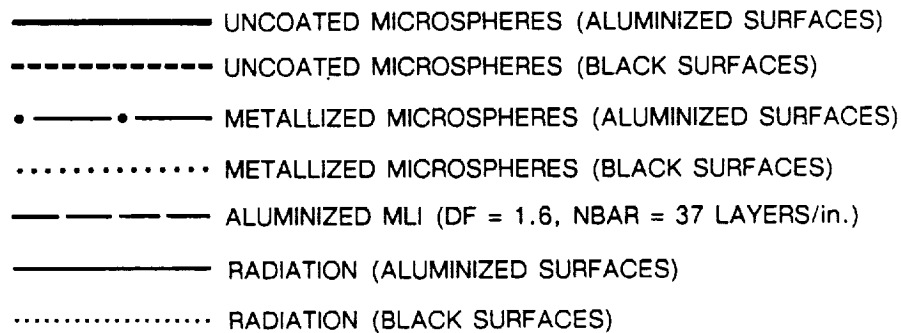


Fig. 2-10 Comparison of Microsphere and MLI Performance Predictions

## Section 3

### EXPERIMENT DESIGN

#### 3.1 CONCEPTUAL DESIGN

The basic measurement of the experiment will be to apply a known heater power ( $Q$ ) to an insulation's test space and measure the temperature difference ( $\Delta T$ ) across the insulation test space at steady-state conditions. The performance will be determined by the thermal resistance ( $R$ ) according to the following linear heat conduction equation:  $R = \Delta T/Q$ .

#### 3.2 PRELIMINARY EXPERIMENT DESIGN CONCEPT

Figure 3-1 shows the preliminary experiment design concept. The experiment configuration contains an aluminum block (6063-T6) with nine 1.5-in.-diameter holes bored into it to form cavities. A 1.0-in. O.D. aluminum tube with a 0.050-in. wall is centered in the cavity, with low-conductance composite tubes at each end. These thermal isolators are 3 in. long, with a 0.9-in. I.D., and are assumed to be as thin as possible (0.005 in.) to provide maximum thermal isolation from the 2-K cold walls. The insulation is tested in the 0.25-in. space between the cavity wall and center tube. Heat is applied uniformly to the inner tube with the use of thermofoil heaters. The applied heat is conducted through the test insulation over the entire 10-in. length of the central aluminum tube.

A thermal model of this design concept was developed using the thermal analyzer program, THERM. A heat map is shown in Fig. 3-2 for a uniformly distributed heat input of 1 mW. As shown in the heat map, essentially all the input heat is conducted out through the thermal isolators, and not across the insulation test space. This holds true for composites such as fiberglass/epoxy, alumina/epoxy, and graphite/epoxy. Even the use of very low-conductance epoxies without any composite fibers resulted in significant heat losses across the thermal isolators. These large parasitic losses would not allow accurate measurement of microsphere thermal performance, since a small percentage of the input heat goes through the test section. The only way to ensure accurate measurement is to

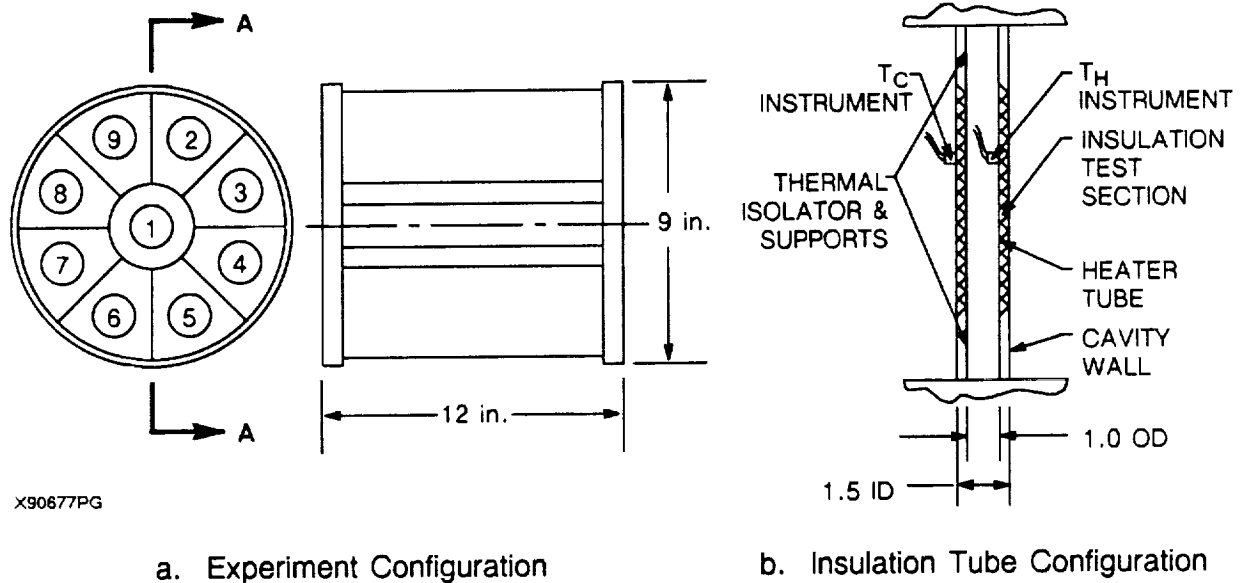


Fig. 3-1 Preliminary Design Concept

significantly reduce the parasitic losses. An effort was made to minimize these losses by varying the length and diameter of the isolators. The thickness was held constant, because it was already as thin as possible. Results indicated that losses could only be reduced to approximately half of the input power, which indicated that the experiment design had to be modified.

### 3.3 EXPERIMENT DESIGN

#### 3.3.1 Design Concept

A revised design was established that incorporated a guard which runs at the same temperature as the test section and greatly reduces the parasitic losses from the test section. The schematic is shown in Fig. 3-3. The design is similar to the preliminary design concept in that it will fit in a 1.5-in. diameter well. A 10-in.-long, 1.0-in.-O.D. aluminum inner tube with a 0.050-in. wall is used as the hot-temperature boundary. This hot-boundary tube is supported from a central aluminum tube by a spoke arrangement of three 0.010-in.-O.D. by 0.005-in.-wall G10 fiberglass/epoxy tubes. This central tube serves as a guard for the

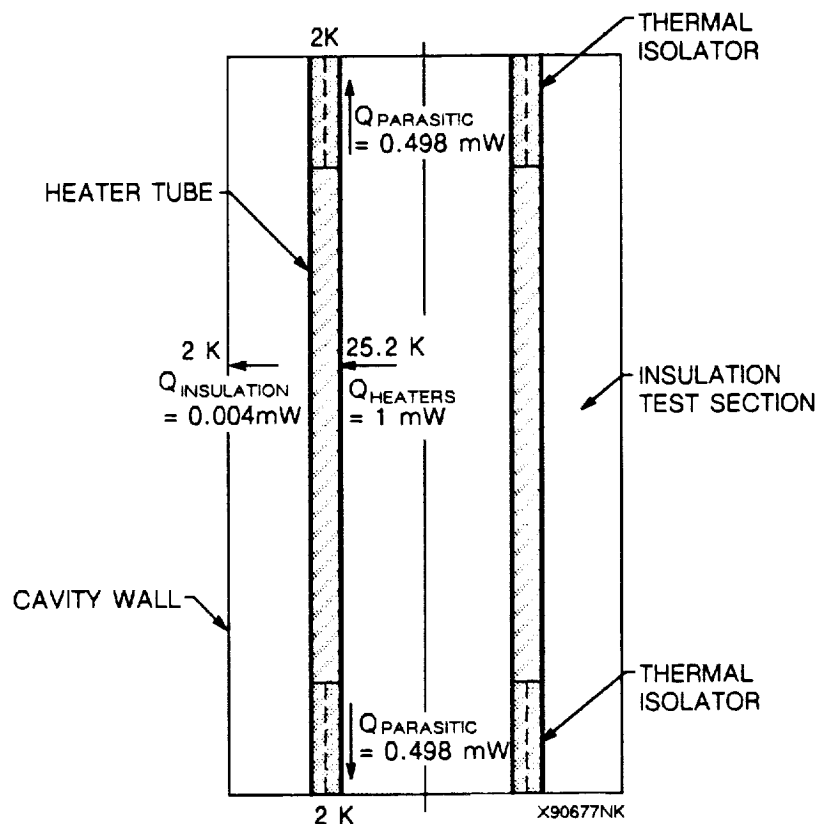


Fig. 3-2 Preliminary Concept Heat Map for Uncoated Microspheres in 0 g

hot-boundary tube by controlling its temperature to that of the test section. This reduces the parasitic losses to an acceptable level. The spokes provide thermal isolation between the hot-boundary tube and the central temperature control section. The entire insulation test cell is supported and thermally isolated from the 2-K wall using a 2.5-in.-long, 0.1-in.-O.D. G10 fiberglass/epoxy tube with a 0.010-in. wall thickness. Thermfoil heaters and silicon diodes are located on the hot-boundary tube and the temperature control section at the point where the spoke standoffs are attached. The hot-boundary tube heaters provide the insulation heat load, while the temperature control heaters are used to match the temperature between the hot boundary and the temperature control section, forming an isothermal cavity. Since essentially no temperature differential will exist across the spoke supports, no heat will be conducted from the hot-boundary tube to the temperature control section, thus ensuring that the heat input to the hot-boundary tube will be conducted through the microsphere insulation. The heater power to the test section and temperature

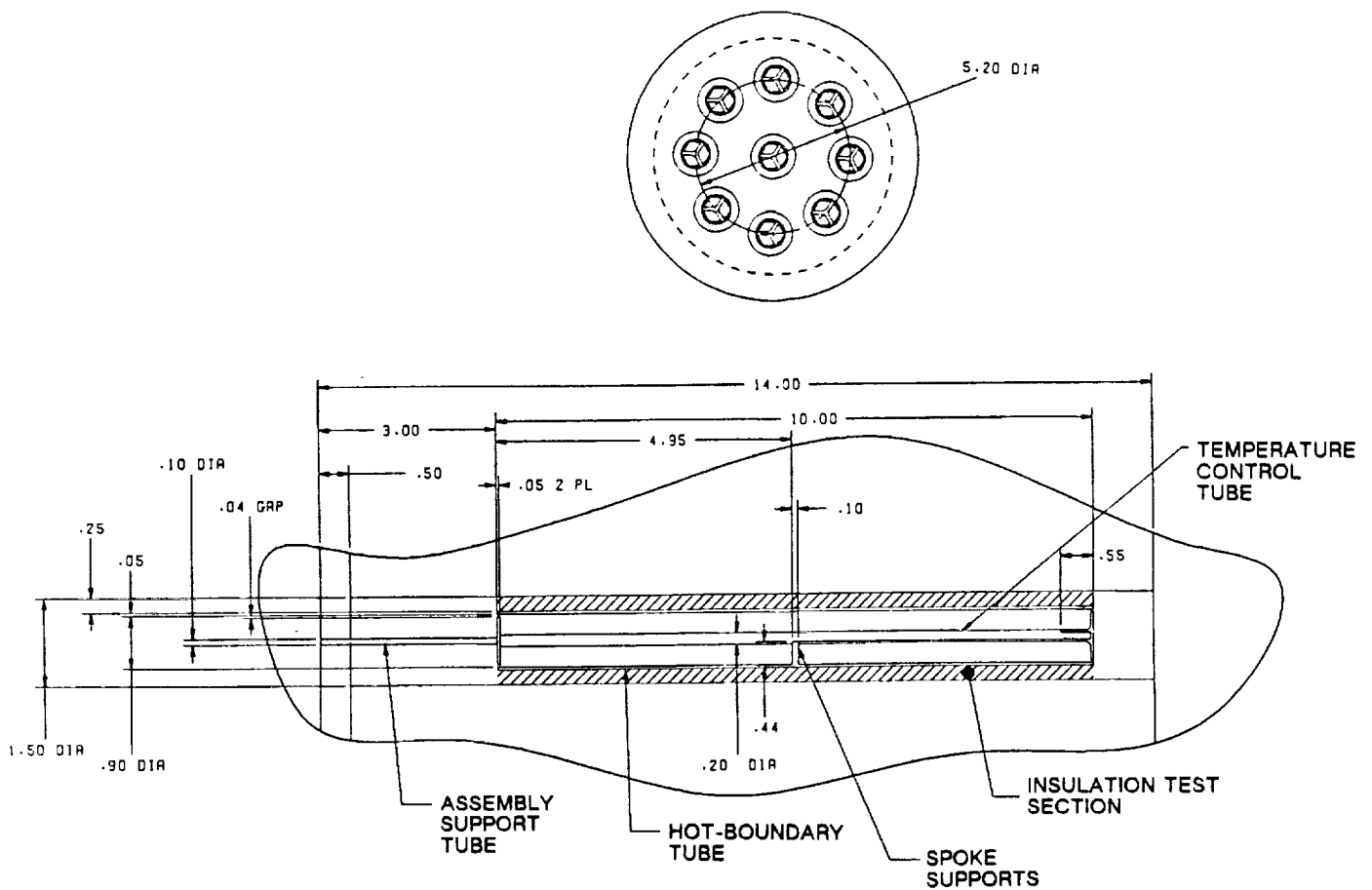


Fig. 3-3 Insulation Experiment Cell

difference across the insulation test section will be measured to calculate the insulation performance (i.e., thermal resistance).

A thermal model was also developed for this design using THERM. A heat map for the system with 1 mW of heat input into the hot-boundary tube is shown in Fig. 3-4. This shows that all of the heat is going across the test section, resulting in a  $\Delta T$  across the insulation space. Power levels of 5 and 10 mW were also investigated, with similar results. Eight 10-mil manganin heater wires and eight 5 mil-manganin diode wires are included in the model. The wires were routed down the single fiberglass/epoxy thermal isolater to the temperature control section with four 20-mil and four 5-mil wires ending at the heater and diode connection points. The remaining wires were routed across the spoke standoffs to

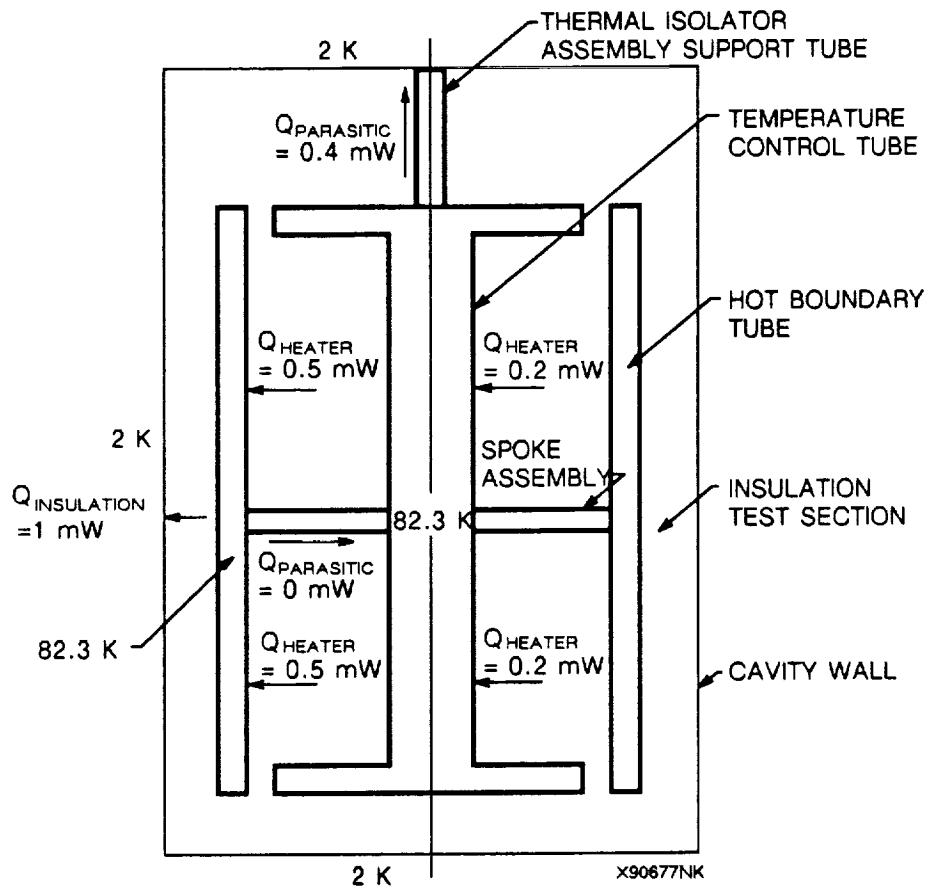


Fig. 3-4 Isothermal Cavity Heat Map for Uncoated Microspheres in 0 g

the other diode and heater connection points. Results evaluated indicate that the design is more than adequate in measuring the thermal performance of microsphere insulation.

The experiment design was sized based on the predicted thermal performance of uncoated glass microspheres in 0-g. The predicted performance is based on the previous work done with glass microspheres (Ref. 1). Various trade studies were done to determine the variation of microsphere performance due to changes in the experiment design. Figures 3-5 and 3-6 show the effect on microsphere resistance of changing the outer diameter or length of the hot-boundary tube, respectively. Figure 3-7 shows the effect on thermal resistance of varying the insulation test section thickness for both uncoated and metallized microspheres. The baseline values have been selected in an effort to have a low thermal resistance within reasonable dimensions and tolerances. A low thermal

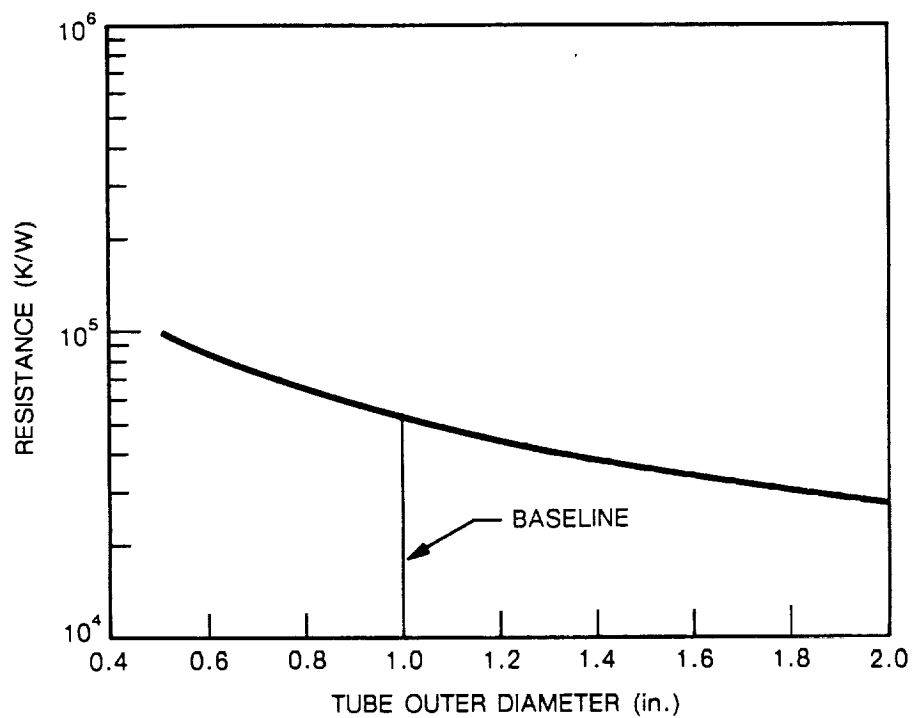


Fig. 3-5 Effect of Hot-Boundary Tube Diameter on Microsphere Resistance

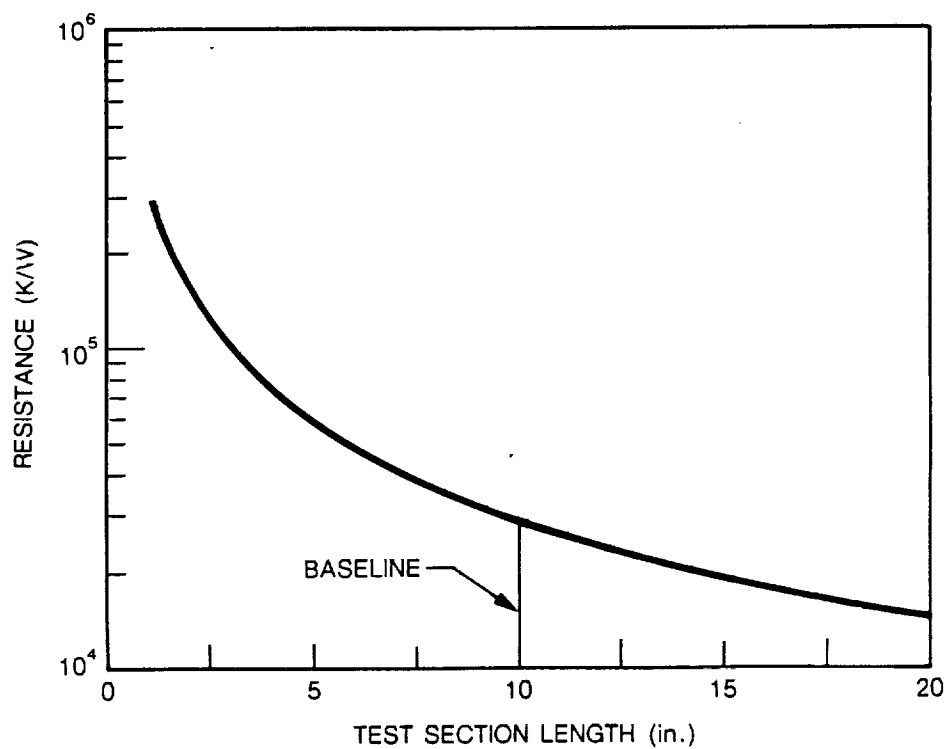


Fig. 3-6 Effect of Insulation Test Section Length on Microsphere Resistance

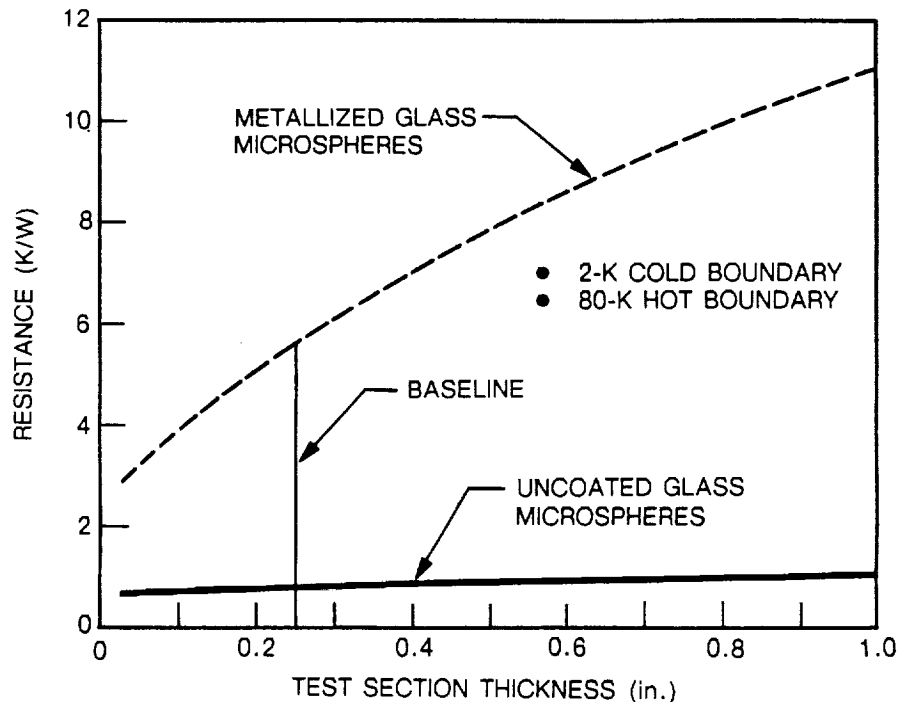


Fig. 3-7 Effect of Insulation Test Section Thickness on Microsphere Resistance

resistance should simplify the measurement and reduce the insulation time constant so that more data can be taken.

### 3.3.2 Performance Characteristics

The main aluminum body currently contains nine wells for insulation testing. The tests will include evaluating the thermal performance of both uncoated and metallized microspheres for various boundary emissivities. Their performance will also be evaluated over a range of hot boundary temperatures. These results will be compared to reference insulation such as MLI and low-emissivity radiation surfaces. Predicted experimental test conditions for these insulations are shown in Fig. 3-8. This figure shows the predicted range of heater powers required for the different insulation systems.

A transient thermal model was developed for the experiment using THERM. The model included transient control logic to simulate the test section temperature response and power requirements. The transient behavior is of interest because it will affect the operation of the experiment. The amount of time required to reach steady-state conditions

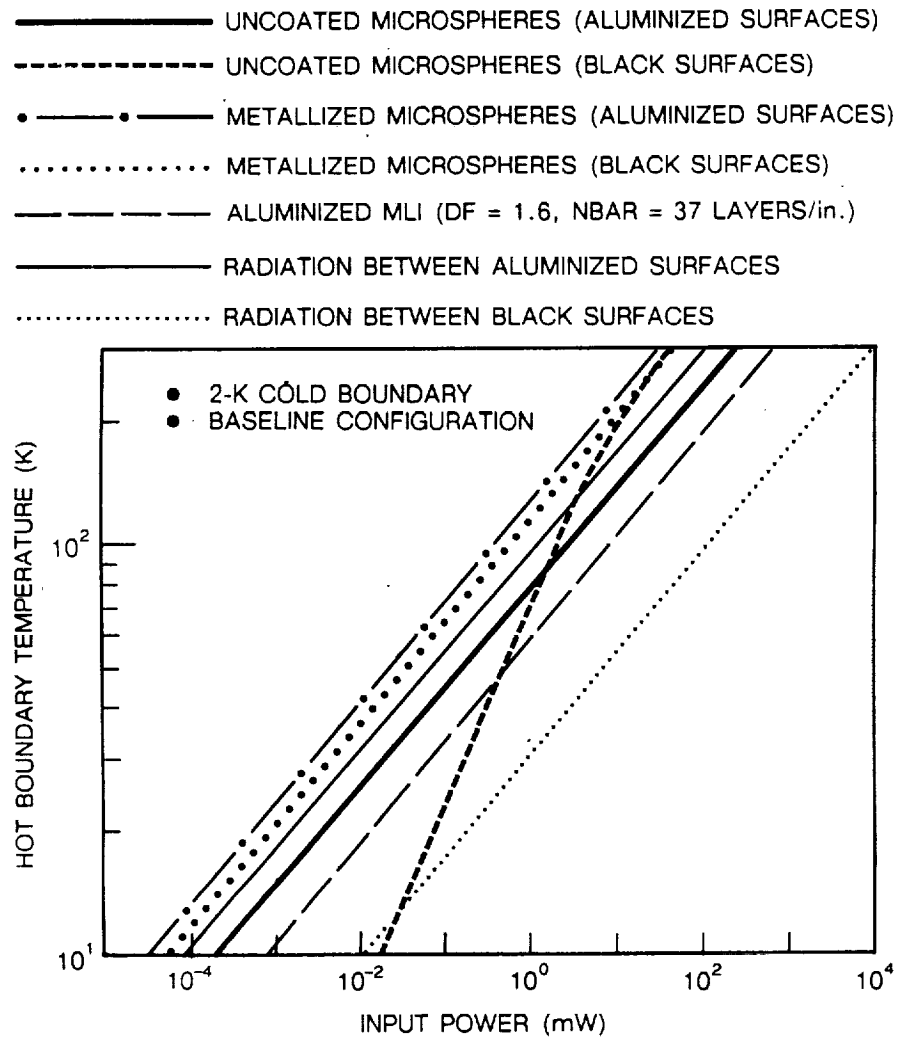


Fig. 3-8 Comparison of Insulation Performance Predictions

will affect the number of data points (different hot temperature boundaries) that can be taken during a sortie mission. The transient response of the experiment test section from 2 to 300 K for both metallized and uncoated microsphere insulations is shown in Figs. 3-9 and 3-10, respectively. The figures show that it is possible to influence the time required to reach steady state with variable input heat. The heater power would be high at first to decrease the time required to warm up to the next boundary temperature. As the desired boundary temperature is approached, the heater power would be reduced to maintain a constant hot boundary temperature. Figure 3-11 compares the transient response of the heaters on the hot-boundary tube and the central temperature control tube for both metallized and uncoated microsphere insulation. It is the test section heater response that determines when steady state exists. For metallized microspheres initially at 2 K, it takes 800 min to reach a steady-state condition with a 300-K hot boundary and a 2-K cold boundary. The uncoated microspheres reach steady state after 250 min.

The proposed test sequence transient response is shown for both metallized and uncoated microspheres in Figs. 3-12 and 3-13, respectively. Data would be obtained at 50-, 100-, 150-, 250-, and 300-K hot boundary temperatures over 4 days. Data at any one

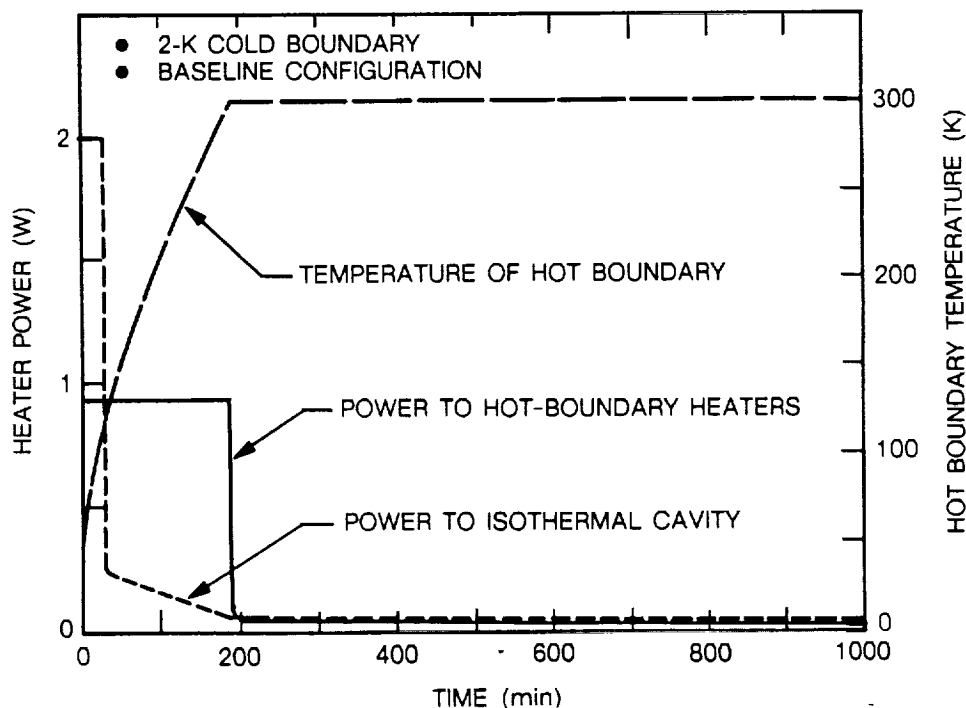


Fig. 3-9 Transient Response of Metallized Microspheres

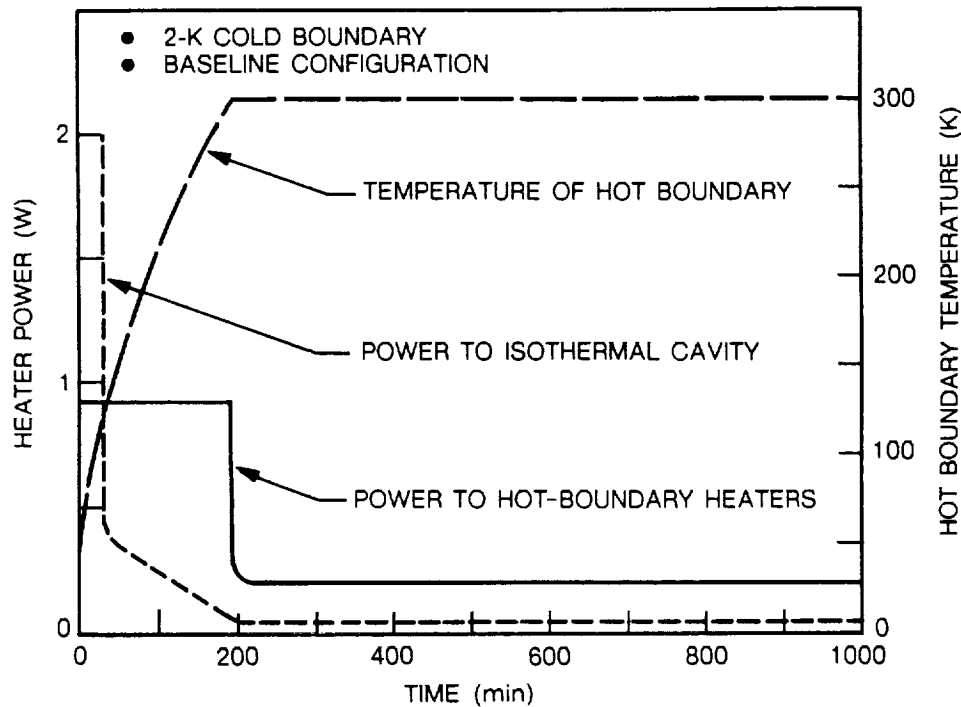


Fig. 3-10 Transient Response of Glass Microsphere

temperature would be recorded for 16 h after the hot boundary tube temperature and heater power have stabilized.

A temperature difference between the hot boundary and the temperature control tube would result in a parasitic heat load that will affect the amount of heat going across the insulation test section. This would result in an error in the resistance calculation. The thermal model of the experiment test cell was used to determine the sensitivity of this heat flow to a temperature difference between the two sections. Figures 3-14, 3-15, and 3-16 show the ratio of input heater power to actual heater power ( $Q_{\text{actual}} = Q_{\text{input}} + Q_{\text{parasitic}}$ ) as a function of the temperature difference between the two sections. These figures show the temperature control requirement to achieve a particular experimental accuracy.

Figure 3-14 illustrates how sensitive the metallized microsphere results are due to their relatively high resistance under 0-g conditions. Their sensitivity to the temperature difference increases for decreasing hot boundary temperature. For temperatures below 100 K, the temperature control must be extremely accurate in order to obtain meaningful results. Figure 3-15 shows that the glass microspheres are less sensitive under the same conditions. Uncoated microspheres in 1-g are relatively insensitive to the temperature

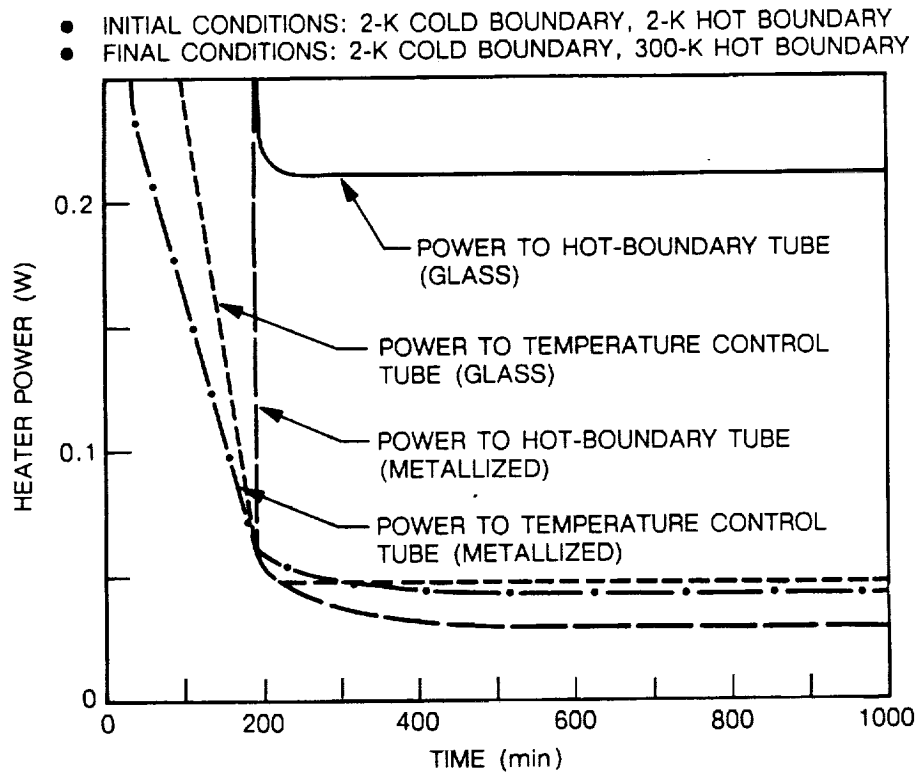


Fig. 3-11 Power Required to Warm Microsphere Test Setup

difference between the test section and the central temperature control section, as shown in Fig. 3-16.

### 3.4 GROUND TEST

#### 3.4.1 Ground Test Design

A single test cell containing glass microspheres was constructed according to the drawings shown in Figs. 3-17 through 3-19. The main purpose of this test was to verify the design concept of the isothermal cavity by maintaining temperature control from one data point to the next, determine the time required to reach steady-state conditions, and obtain some actual thermal performance data on uncoated glass microspheres in 1 g. The test was performed using liquid nitrogen instead of liquid helium due to cost and time considerations.

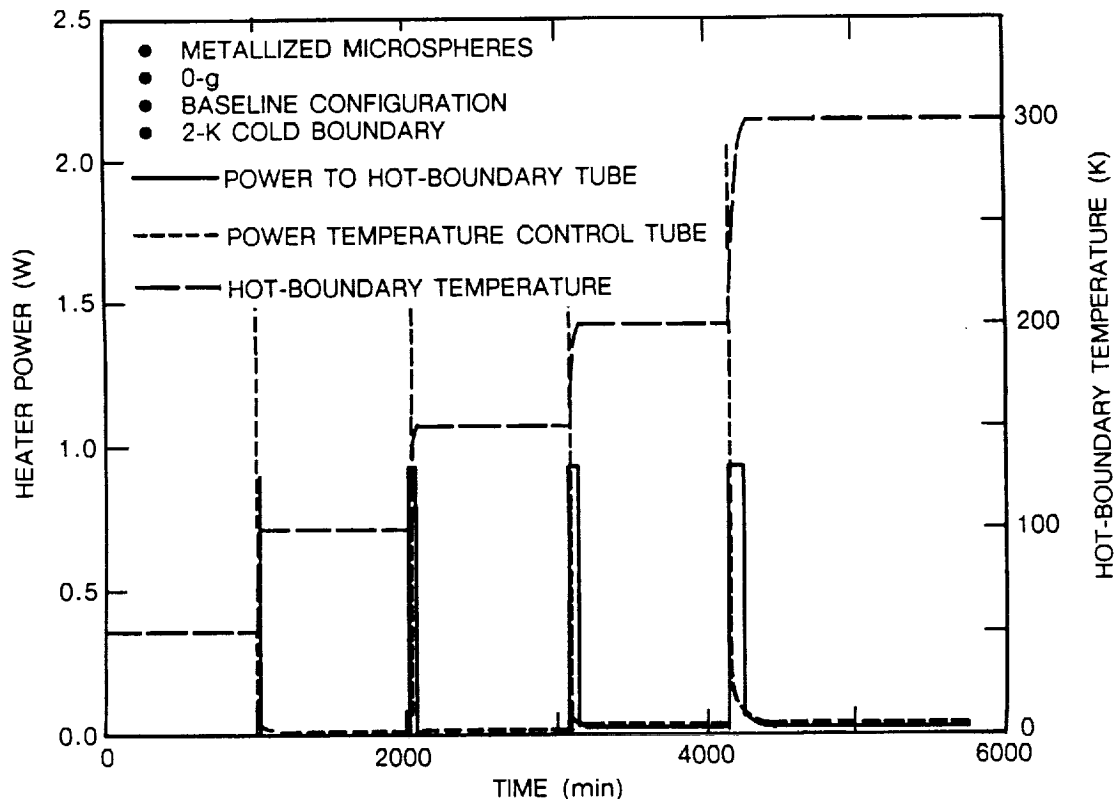


Fig. 3-12 Proposed Microsphere Test Sequence Transient Response for Metallized Microspheres

The ground test cell is exactly as proposed for the flight experiment, except that the cold-boundary well was simulated by a 1.5-in.-I.D., 0.5-in.-thick wall 6061-T6 aluminum tube. The hot-temperature boundary is a 10-in.-long, 1.0-in.-O.D. aluminum tube (6061-T6) with a 0.050-in.-thick wall (Fig. 3-20). The central tube forming the inner section of the isothermal cavity is a 6061-T6, 0.20-in.-O.D. rod with a 0.50-in.-O.D., 0.050-in. thick disk at one end. The other end is threaded for attachment of a second 0.50-in.-O.D., 0.050-in.-thick disk (Fig. 3-21). These disks are the same O.D. as the hot-boundary tube and enclose the ends of the tube to reduce end-loss effects. The central temperature control tube is suspended from the cold boundary by a single 2.5-in.-long, 0.1-in.-O.D., 0.010-in.-thick wall G10 fiberglass/epoxy tube (Fig. 3-22). The hot-boundary tube is supported and thermally isolated from the central tube by three 0.10-in.-O.D., 0.005-in.-thick wall G10 fiberglass/epoxy tubes (Fig. 3-23). Thermofoil heaters and silicon diodes were used on the central tube and hot-temperature boundary for temperature control and thermal performance measurements; 5- and 10-mil manganin wire was used

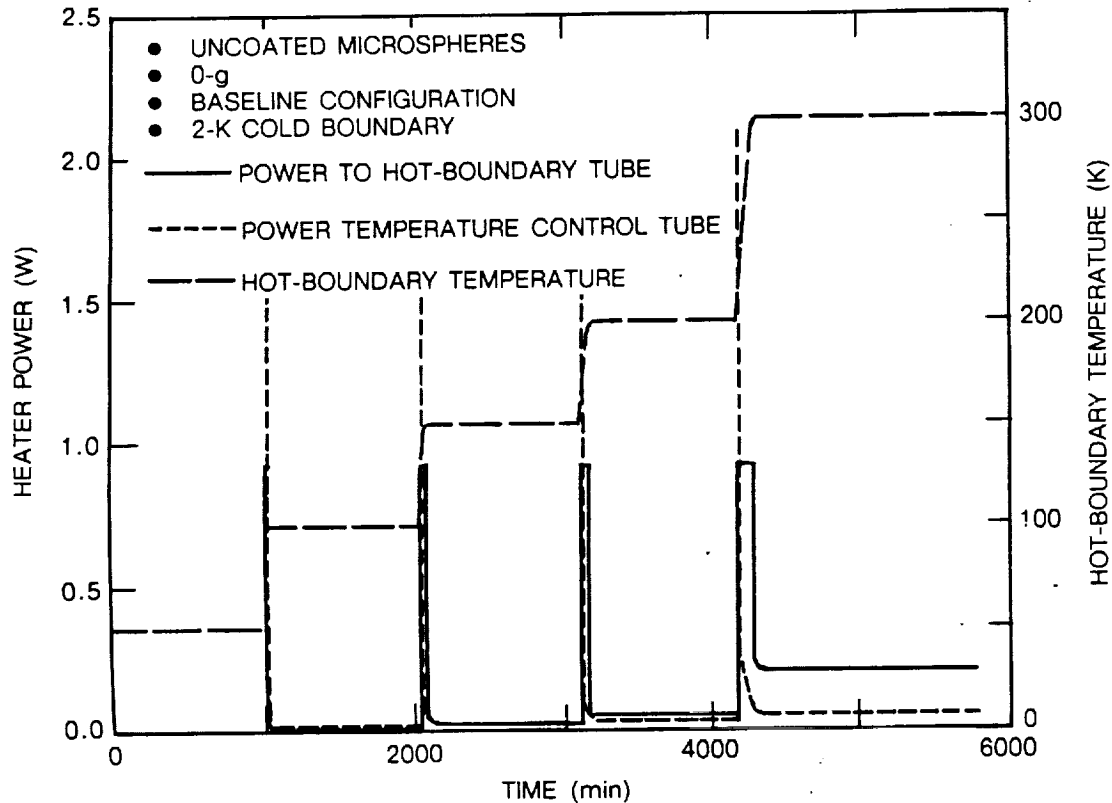


Fig. 3-13 Proposed Microsphere Test Sequence Transient Response for Uncoated Microspheres

for the silicon diodes and heaters. These wires were routed down the 2.5-in.-long fiberglass support tube to individual feedthroughs in one end of the cold boundary well. The other end of the well contained a 0.5-in.-O.D. 20- $\mu$ m stainless steel porous plug which was used to evacuate the microsphere insulation (Fig. 3-24).

### 3.4.2 Test Article Fabrication and Assembly

After all of the components were machined, a single Lake Shore Cryotronics DT-470-SD-11 silicon diode was installed onto the central temperature control tube and onto the hot-temperature boundary tube (Fig. 3-25). The 2.5-in., 0.1-in.-O.D., 0.010-in.-thick walled fiberglass tube was then bonded to the end of the central tube and the cold boundary well end cap. Sixteen individual electrical feedthroughs were also epoxied into the well end cap. Two Minco thermfoil heaters (HK-5261- R135-L12-A) were bonded at each end of central temperature control tube and connected in series, for a total resistance of  $\sim 270 \Omega$  (Fig. 3-26). Three Minco heaters (HK-5263-R280-L12-A) were

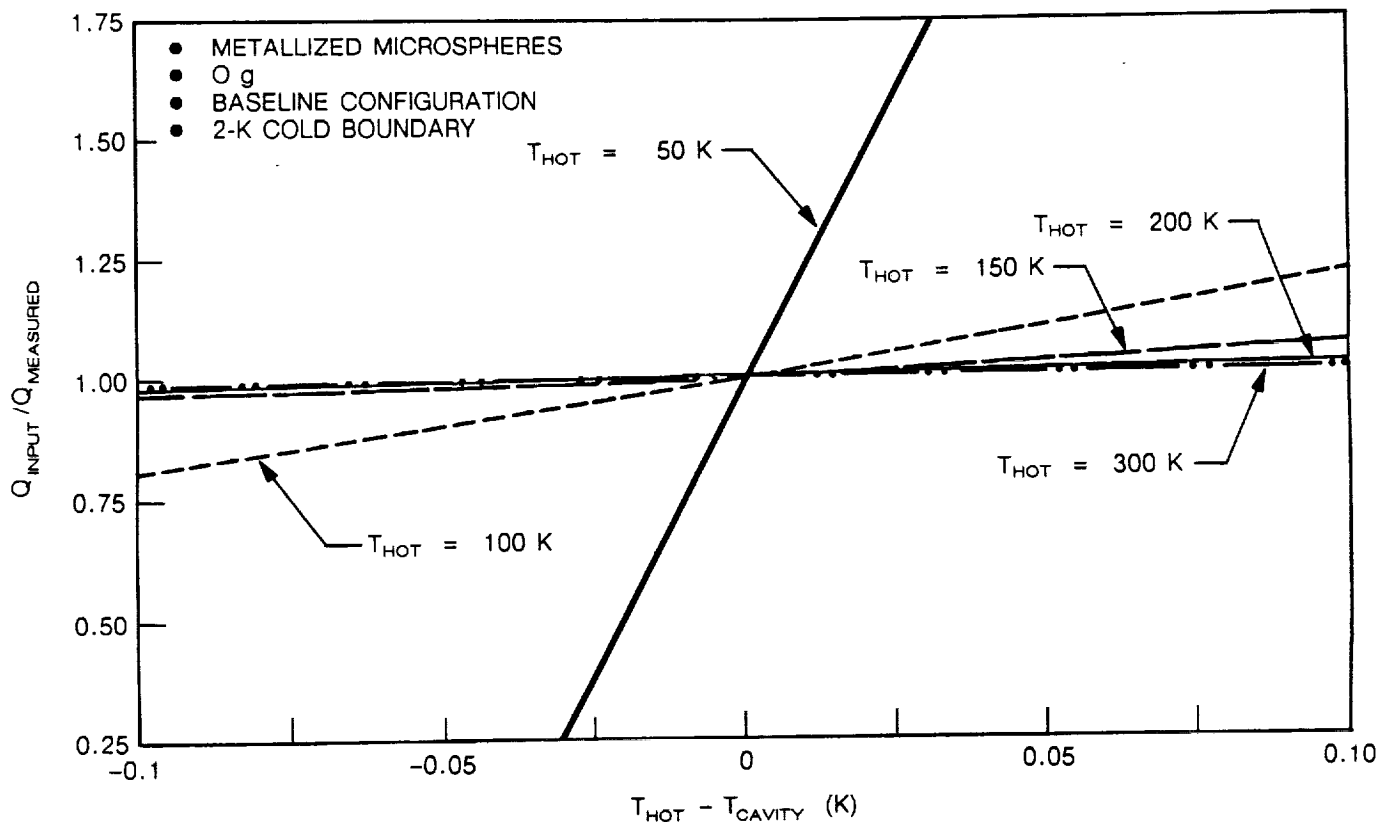


Fig. 3-14 Sensitivity of Heat Rate Measurements to Isothermal Cavity Temperature Differentials, Metallized Microspheres in 0 g

bonded symmetrically around the circumference of the hot-boundary tube along its length, also connected in series, for a total resistance of  $\sim 840\ \Omega$ .

An aluminum doubler was epoxied over the heaters to ensure uniform heating. Twelve 5-mil manganin wires and four 10-mil manganin wires were connected to the cold boundary well end cap feedthroughs and routed through two holes in the end disk of the central temperature control tube (Fig. 3-27). All of the wires were epoxied to the central tube. The central-tube silicon diode was wired with four of the 5-mil manganin wires for current and voltage measurements. Two of the 5-mil wires were connected to the heater on the tube for voltage measurements with two 10-mil manganin wires connected to supply the operating voltage and carry the current. The remaining six 5-mil wires and two 10-mil wires were routed through the central hole as shown in Fig. 3-28. These wires were passed through the inside of the hot-boundary tube and up through its central hole as

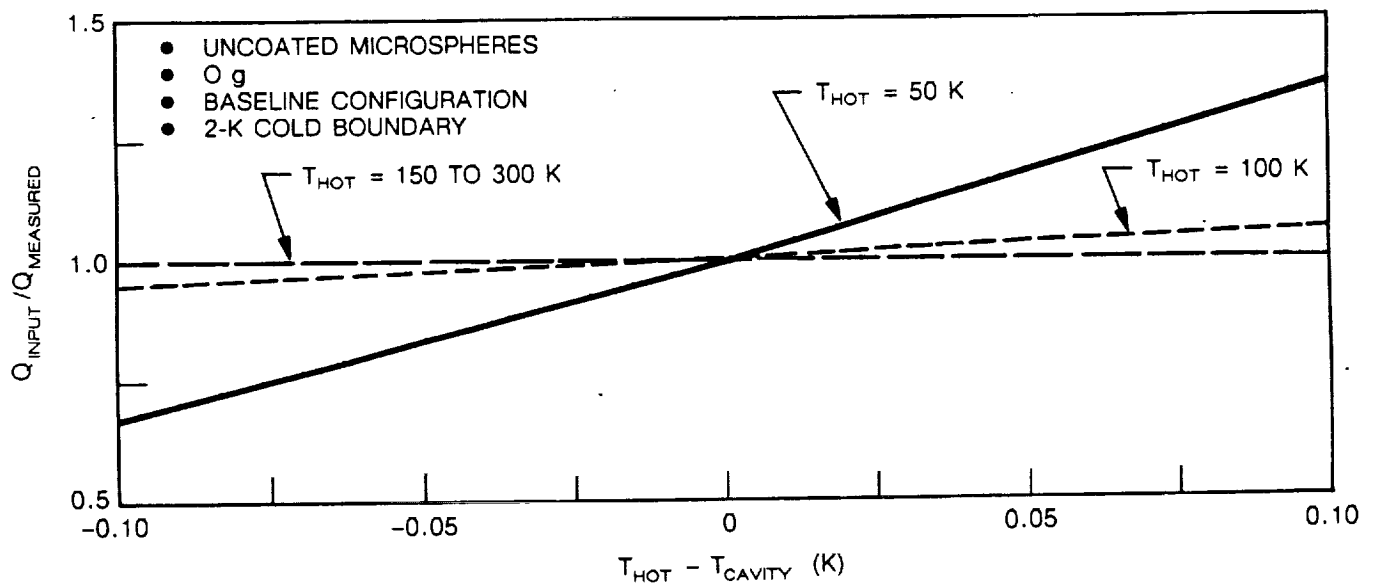


Fig. 3-15 Sensitivity of Heat Rate Measurements to Isothermal Cavity Temperature Differentials, Uncoated Microspheres in 0 g

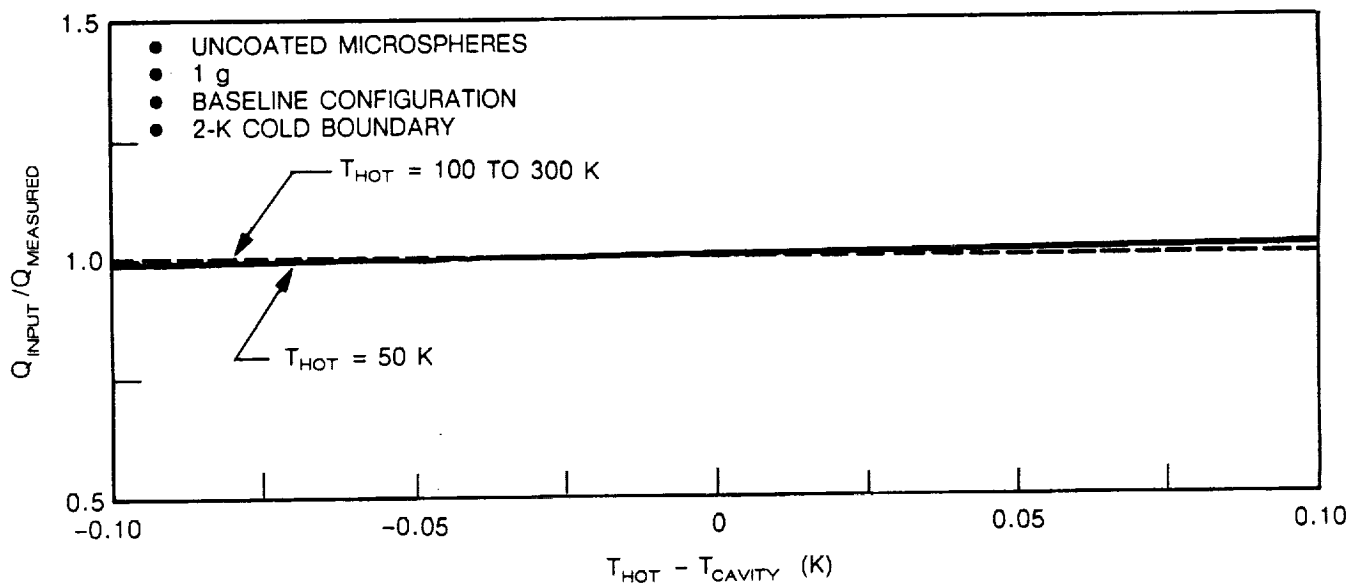


Fig. 3-16 Sensitivity of Heat Rate Measurements to Isothermal Cavity Temperature Differentials, Uncoated Microspheres in 1 g



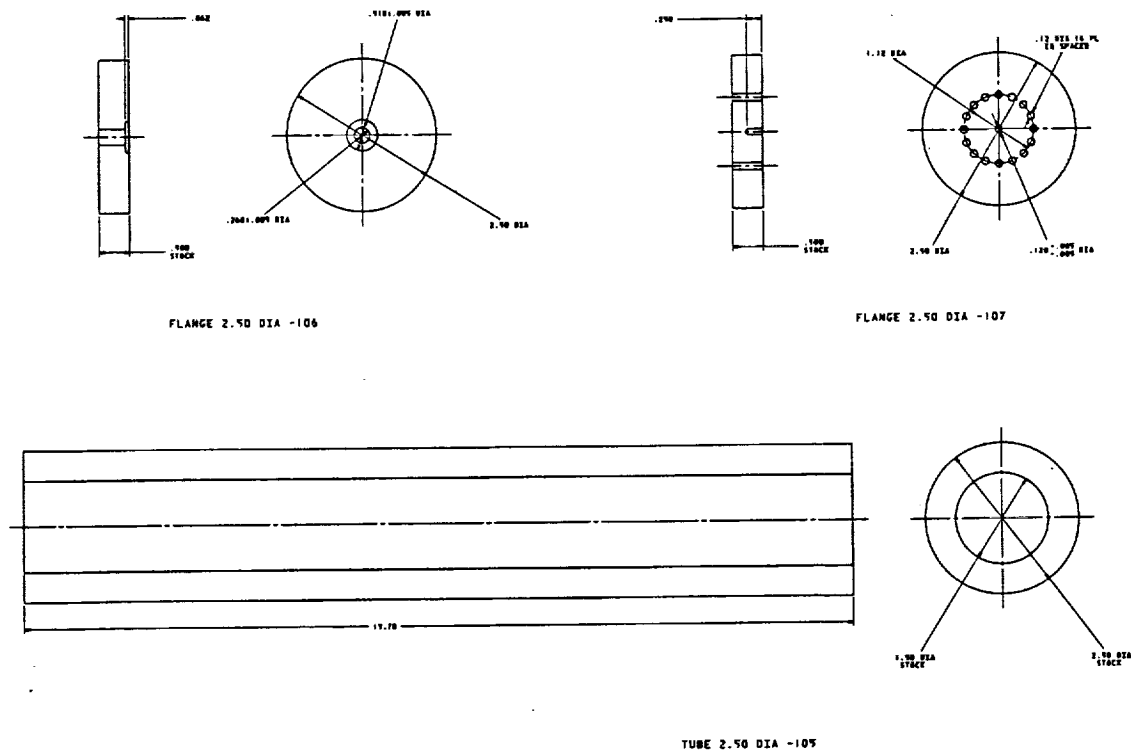


Fig. 3-18 Test Article Vacuum Enclosure

shown in Fig. 3-29. The hot-boundary tube slipped over the central isothermal cavity tube while pulling on the eight wires through the central hole. The entire assembly was placed on end, and the hot-boundary tube was adjusted so that it was 0.050 in. from the central-tube disk and centered about the central tube.

The hot-boundary support tubes were epoxied in the three holes to form the spoked stairway support/thermal isolation system (Fig. 3-30). The wires to the hot boundary were fed through the middle support tube during the bond operation to complete the assembly. The end disk was screwed onto the end of the central tube and adjusted to form a 0.050-in. gap from the hot-boundary tube. This adjustment utilized two 0.050-in. shims which applied pressure to the hot-boundary tube and kept the assembly centered until the

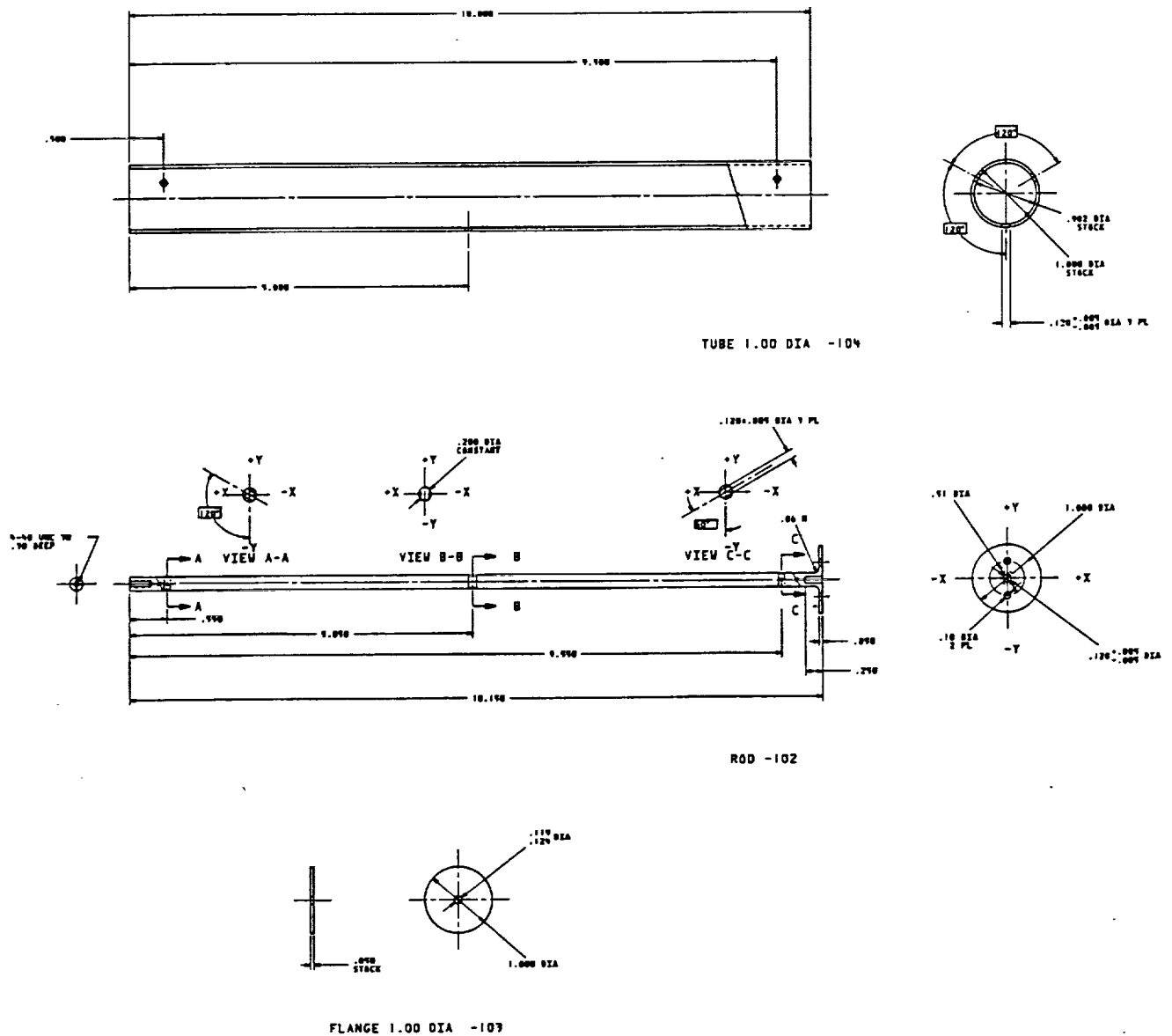


Fig. 3-19 Test Article Internal Components

ORIGINAL PAGE IS  
OF POOR QUALITY

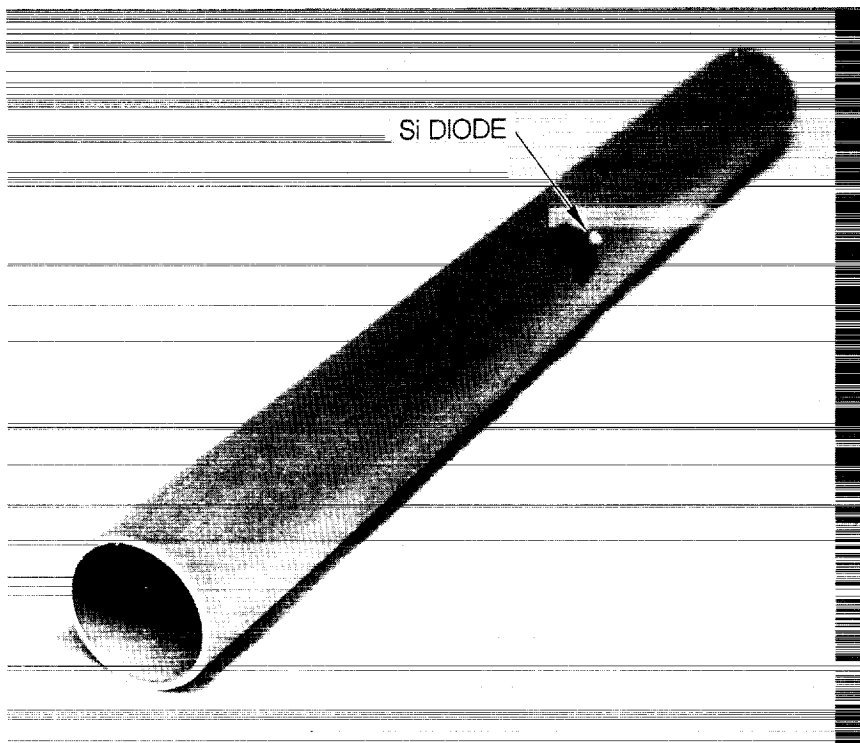
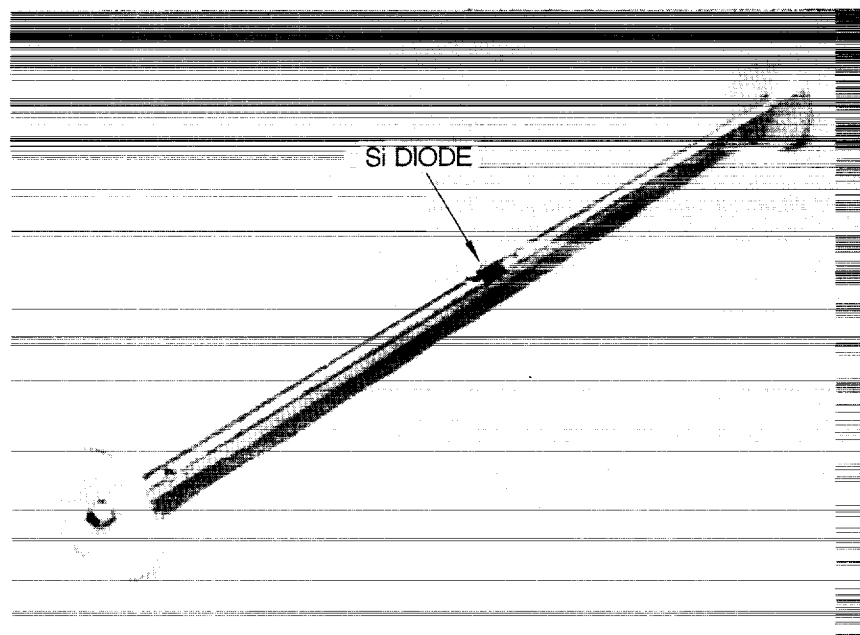


Fig. 3-20 Hot-Temperature Boundary Tube

Fig. 3-21 Central Temperature Control Tube  
and End Disks

0.1-in. O.D.  
0.01-in.-THICK WALL

ORIGINAL PAGE  
BLACK AND WHITE PHOTOGRAPH

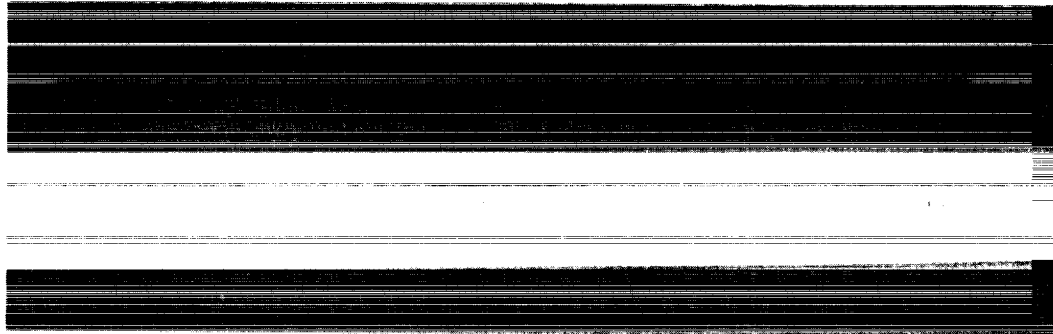


Fig. 3-22 Central Tube Support Tube

0.1-in. O.D.  
0.005-in.-THICK WALL

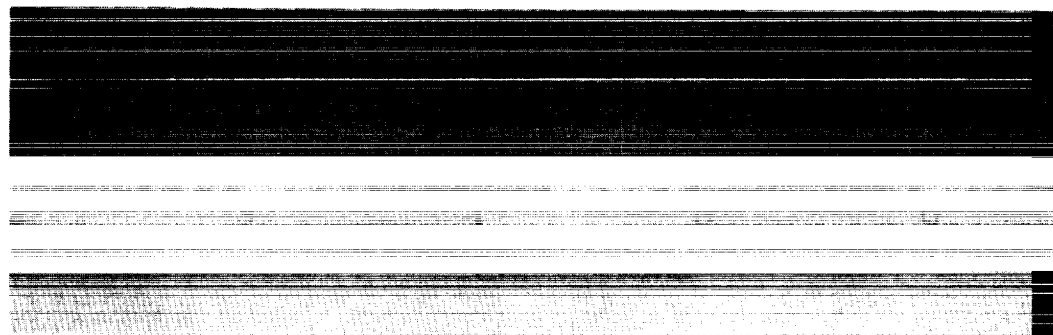
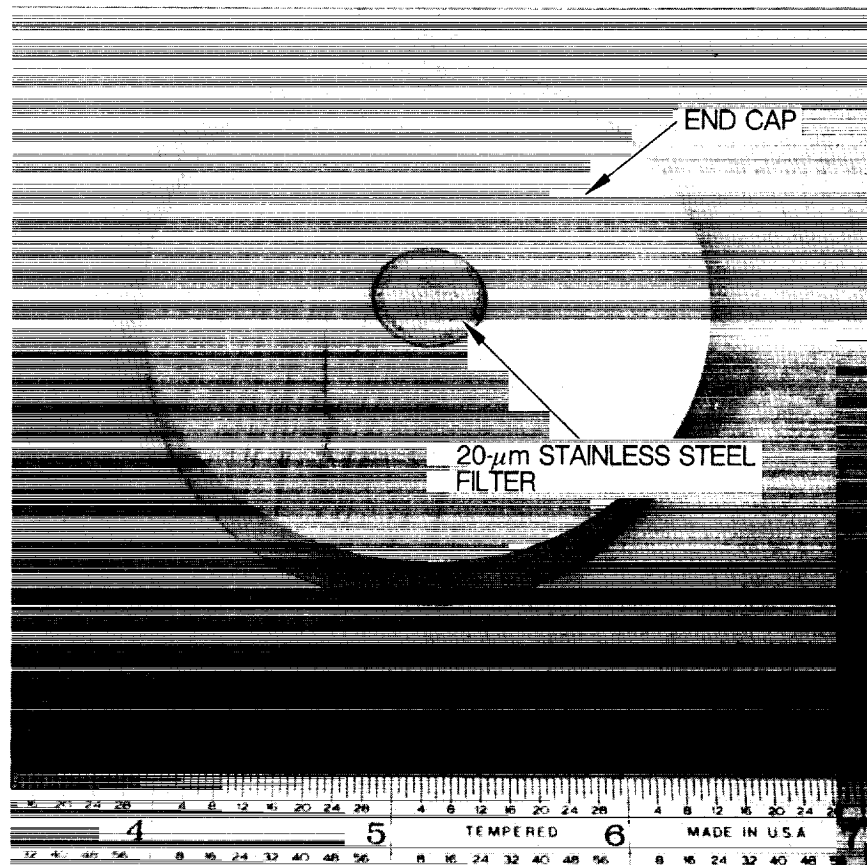


Fig. 3-23 Hot-Boundary Support Tube

epoxy was cured. Four of the 5-mil manganin wires were connected to the silicon diode on the hot-boundary tube. The two remaining 5-mil wires and the two 10-mil wires were connected to the heater. All of the wires were epoxied to the hot-boundary tube for thermal grounding. The completed internal assembly is shown in Fig. 3-31.

A single layer of double aluminized mylar was wrapped around the hot-boundary tube and on the inside of the cold-boundary well to provide low-emittance boundaries (Fig. 3-32). The internal assembly was inserted into the cold-boundary well, and the end cap was epoxied to the well. After the epoxy had cured, the assembly was turned upside down and filled with microspheres (Fig. 3-33). Microspheres were placed in a water tank to allow the broken ones to sink to the bottom of the tank. The unbroken microspheres were baked at

Fig. 3-24 20- $\mu$ m Filter

500 K to remove the water. The assembly was filled with these microspheres (both inside the isothermal cavity and around the hot-boundary tube) up to the end of the central tube. The end disk was attached, and the assembly was completely filled. During the fill process, the assembly was periodically shaken to settle the microspheres and minimize the void space. The end cap containing the porous plug and evacuation port was epoxied on to seal the unit. Two 0.020-in.-thick aluminum doublers were installed over each of the end joints to ensure a leak-tight system. The complete assembly is shown in Fig. 3-34.

### 3.4.3 Test Setup

The test cell was connected to a Leybold-Heraeus 360-L turbomolecular pumping station (Fig. 3-35). The test cell instrumentation was connected to a HP 3054A automatic data acquisition system controlled by a HP 9826 computer. The system provided temperature control with the use of two 50-V power supplies. The HP 9826 computer controlled the voltage supplied to the heaters and measured the heater current using two 100- $\Omega$  standard

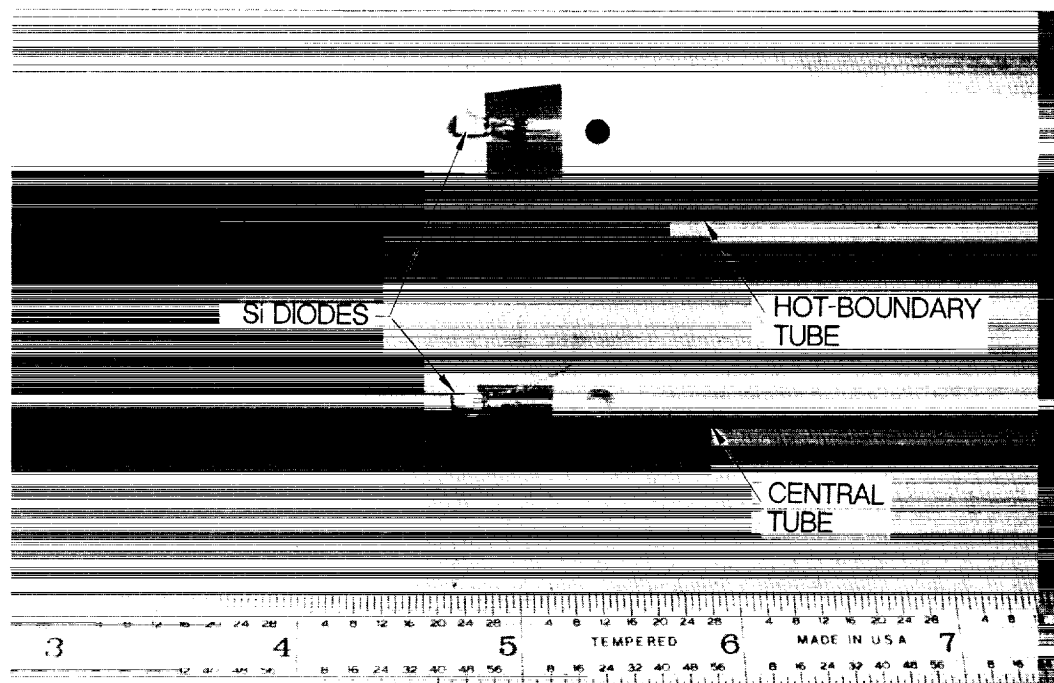


Fig. 3-25 Diode Placement

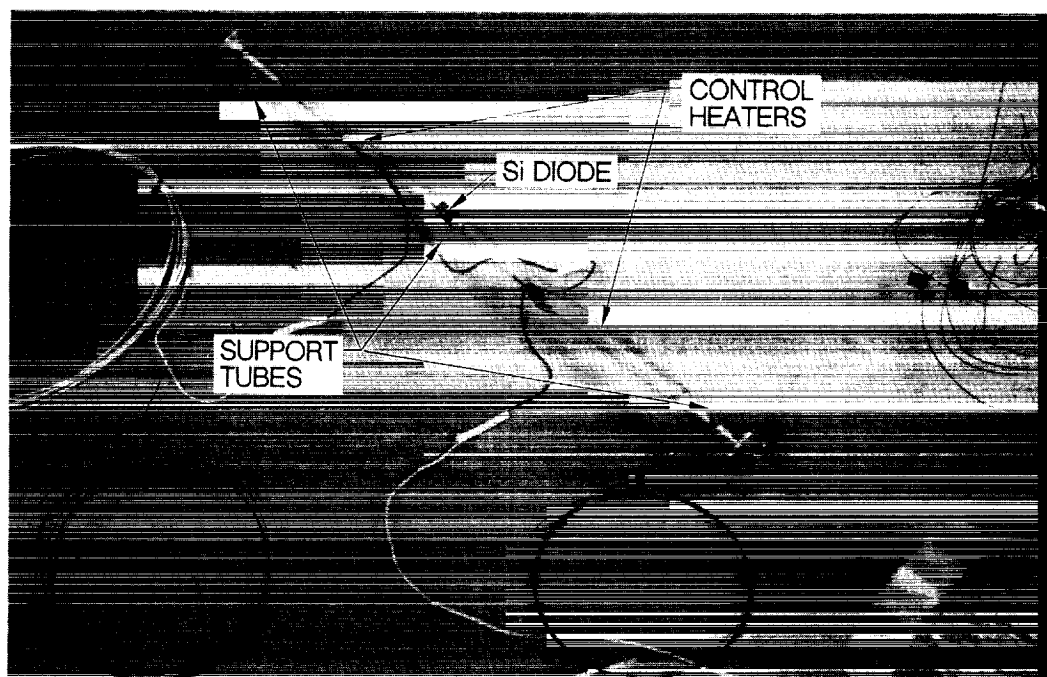


Fig. 3-26 Central Tube Assembly

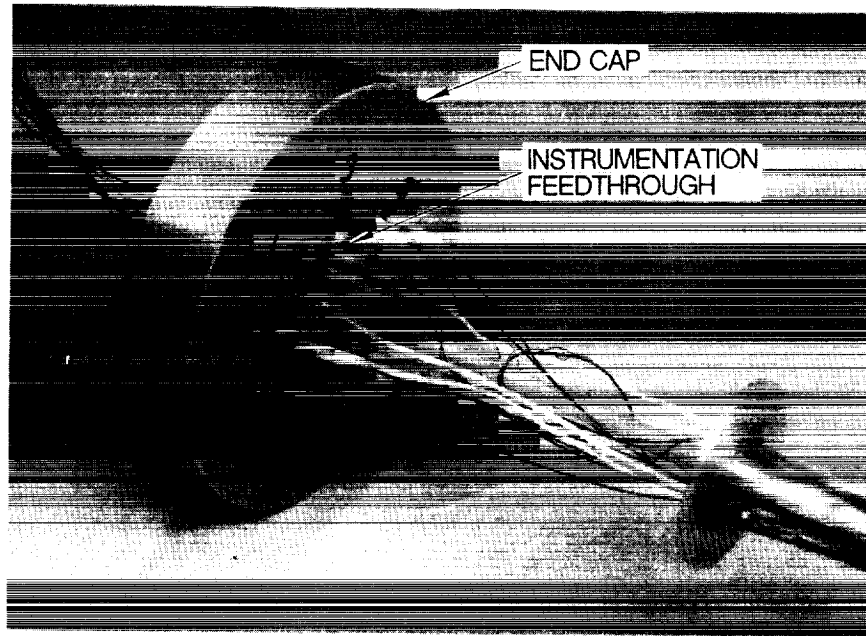


Fig. 3-27 Instrumentation Wiring Through End Cap



Fig. 3-28 Central Tube Instrumentation Wiring

resistors. Temperature was measured by connecting the two silicon diodes in series and using a single LakeShore Cryotronics constant current source to provide  $10\text{ }\mu\text{A}$  of current. Diode voltages were converted to temperatures using Lake Shore Cryotronics Standard Curve No. 10.

The test cell was installed vertically in the open-ended dewar (Fig. 3-36). The pumping station was allowed to evacuate the microsphere test cell for 3 days to provide a vacuum of  $\sim 2 \times 10^{-7}$  torr. The assembly was cooled down by submerging it into a bath of liquid nitrogen and decreasing the pressure to  $\sim 3 \times 10^{-8}$  torr. Temperatures were allowed to stabilize at 78 K before testing began.

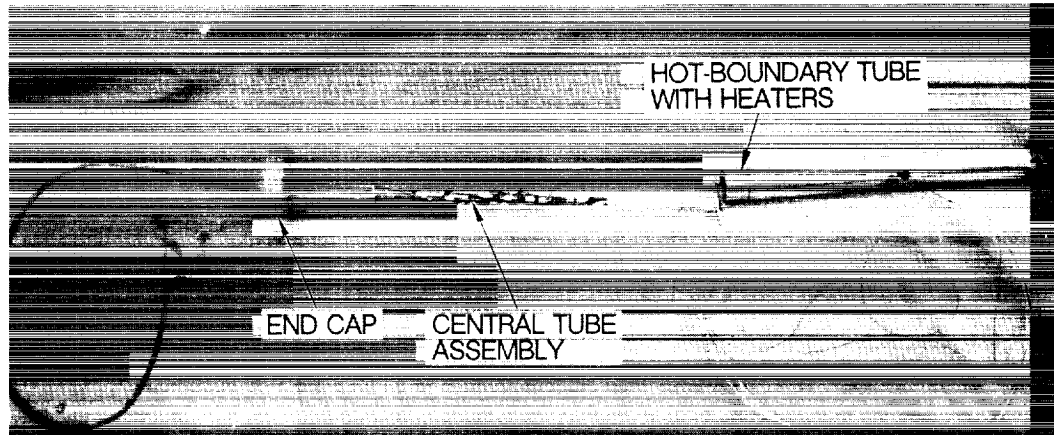


Fig. 3-29 Internal Assembly and Wiring



Fig. 3-30 Internal Assembly, End View

### 3.4.4 Test Results and Conclusions

The thermal performance of microspheres in 1 g was determined for hot boundary temperatures between 85 and 300 K by measuring the heat input to the hot-boundary heater and the temperature difference across the insulation test section. To decrease the time required to reach steady-state conditions going from one hot boundary temperature to

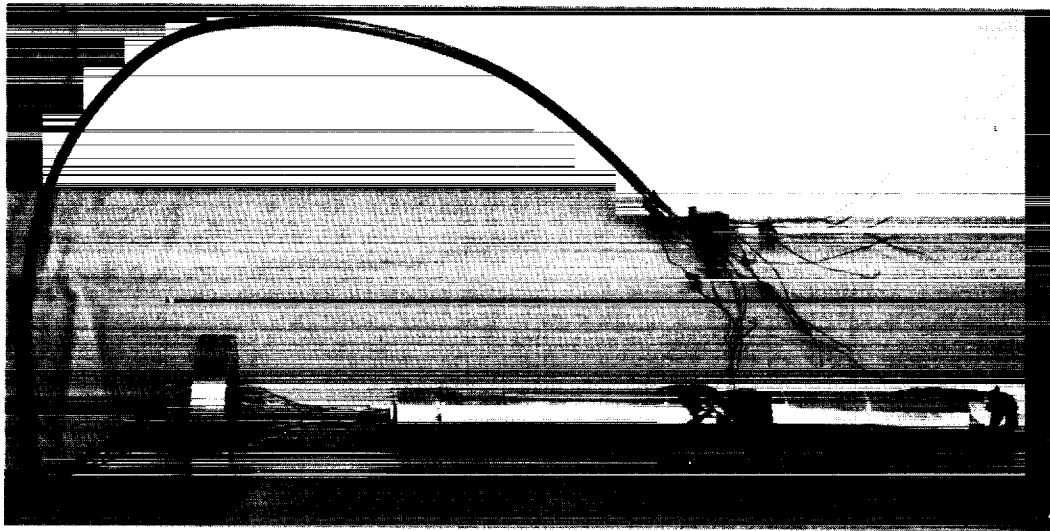


Fig. 3-31 Complete Internal Assembly

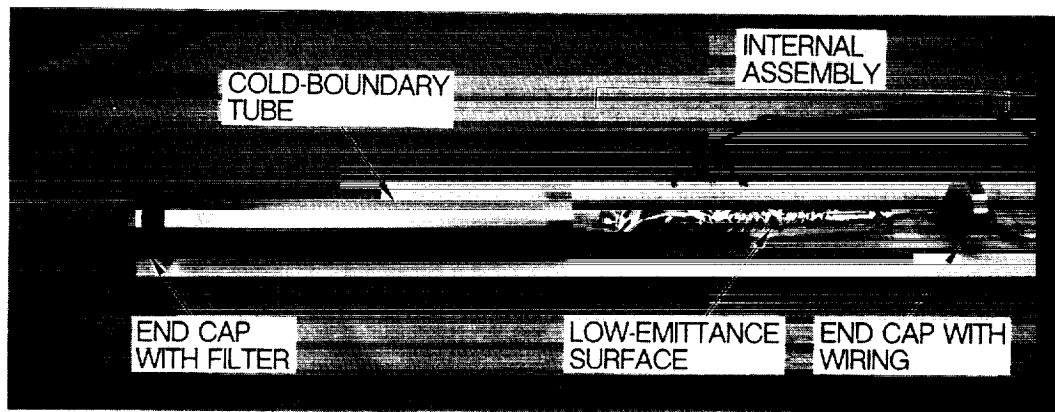


Fig. 3-32 Low-Emittance Hot-Boundary Surfaces

the next, the heater power was increased to a maximum of 2.0 W and then reduced to a steady value as the desired temperature was approached. This control system provides steady-state conditions more quickly than a simple step change in heater power. Steady state was determined by the stability of the hot boundary temperature and heater power. Steady-state conditions were usually observed 4 h after changing heater power to obtain a new hot boundary temperature. The steady-state results are shown in Fig. 3-37 plotted against the predicted performance of uncoated glass microspheres in the test configurations.

ORIGINAL PAGE  
BLACK AND WHITE PHOTOGRAPH



Fig. 3-33 Assembly Filled With Microspheres

The experiment was initially tested at a hot boundary temperature of 100 K. The temperature was increased in subsequent tests by 25-K increments up to 200 K. The data shown for these temperatures were within 25% of predicted microsphere performance. After 200 K, the hot boundary temperature was increased to 250 and 300 K. The data for these two points were 75% higher than prediction and significantly higher than the previous set of data. The system was allowed to cool, and the test with a hot boundary temperature of 150 K was repeated. This result was higher than the previous test at this temperature and 158% higher than prediction. After this test, the system was allowed to cool further, and a test at 85 K was conducted. The resulting data were 80% higher than prediction. The hot-boundary tube was again warmed to 150 K and this temperature was repeated again. The result was between the previous two tests at this temperature and was 60% greater than prediction. The data shown in Fig. 3-35 indicate the direction of temperature change for the system prior to each test.

ORIGINAL PAGE  
BLACK AND WHITE PHOTOGRAPH

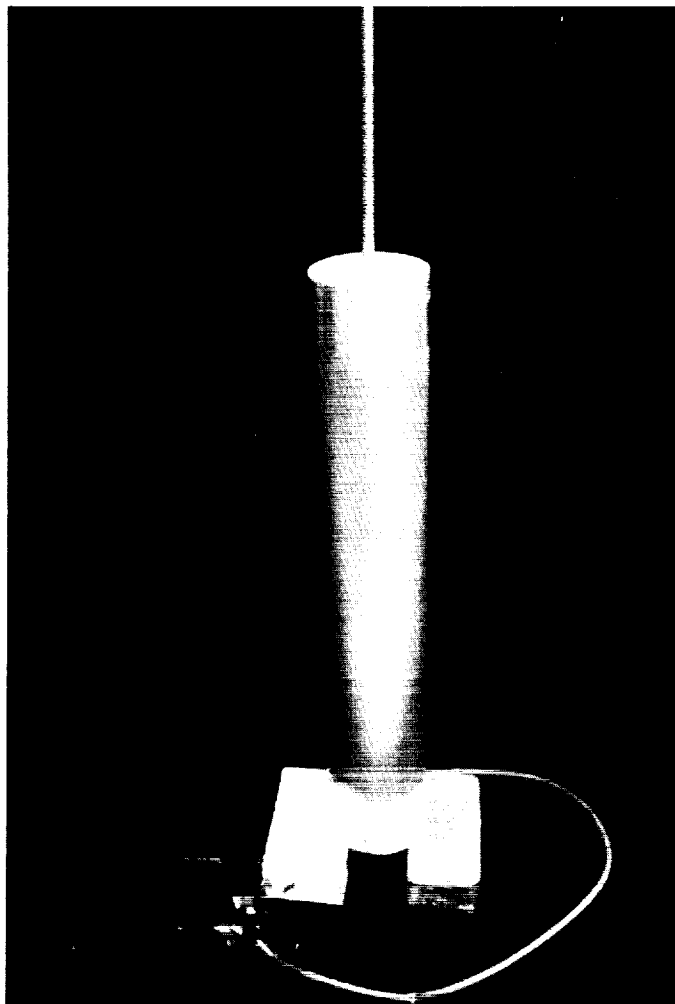


Fig. 3-34 Completed Microsphere 1-g Test  
Assembly

ORIGINAL PAGE  
BLACK AND WHITE PHOTOGRAPH

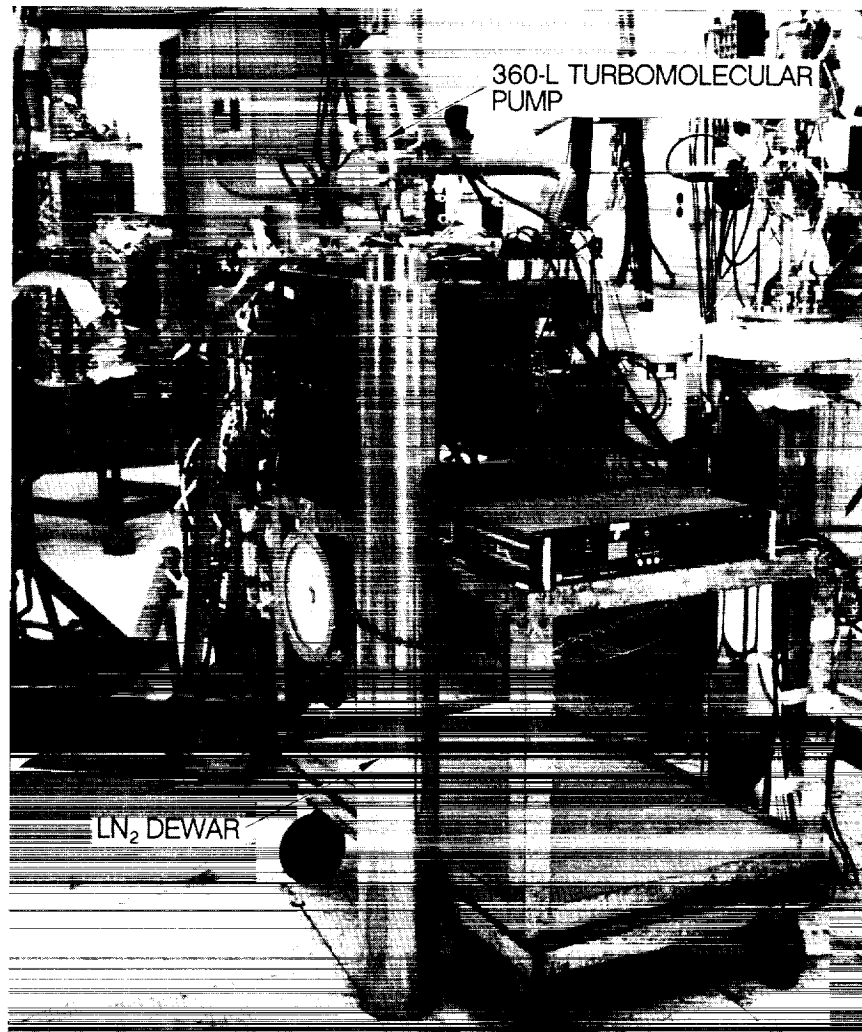


Fig. 3-35 Microsphere Test Setup During Pumpdown



Fig. 3-36 Microsphere Test Assembly Suspended in LN<sub>2</sub> Dewar

Initial data obtained between 100 and 200 K followed the predicted performance curve within 25%. The increased disagreement between test and predicted values in subsequent tests may be due to the larger temperature steps that were used and may have resulted in the microsphere insulation not being in thermal equilibrium during data recording. Another possible explanation could be that the microspheres settled during testing, allowing a radiation coupling to develop between the hot-boundary tube and the cold sink.

Both reasons could explain the discrepancy between the three data points at 150 K. The second data may not have reached steady state after cooling from 300 K, and the microspheres could have been still "soaking out" when the test was changed. The third data point at 150 K appeared to show performance similar to the data at 250 and 300 K (60% versus 75%), which would tend to indicate that something changed within the experiment, such as microsphere settling. This explanation appears likely, since both

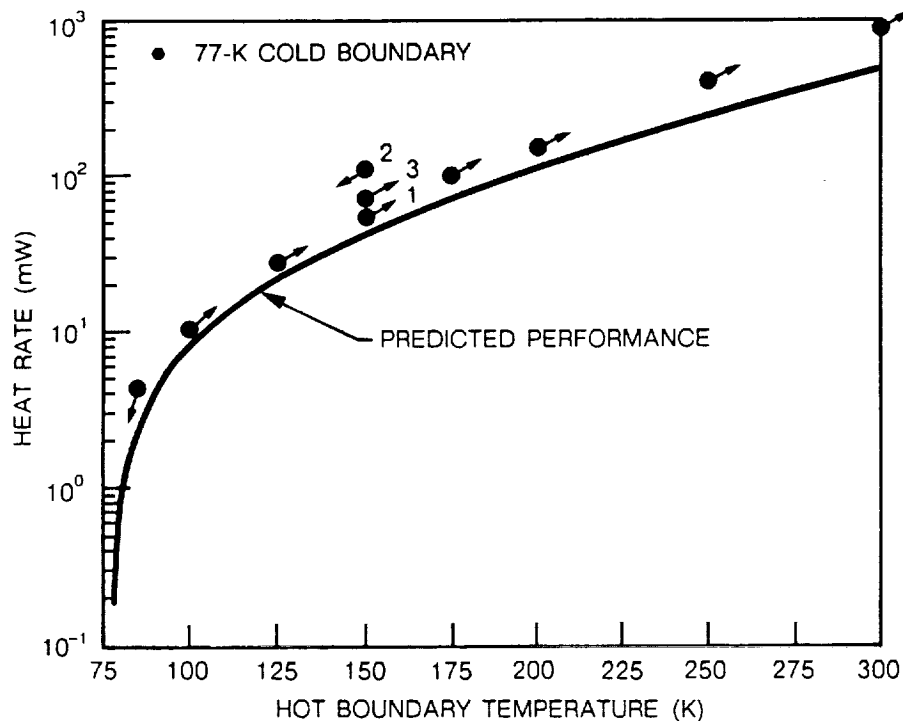


Fig. 3-37 Uncoated-Microsphere Ground Test

hot-boundary tube temperature and heater power were observed to be constant during data recording. Microsphere settling would not be a problem during an orbital experiment due to the lack of gravity. The test cell was not opened for inspection, because future testing with liquid helium was planned. Opening the cell would have damaged the internal epoxy bonds, since it would have been necessary to heat the assembly to break the external epoxy bonds.

### 3.5 FLIGHT EXPERIMENT PACKAGE

#### 3.5.1 Microsphere Flight Experiment

The proposed flight experiment design is shown in Fig. 3-38. The design is composed of nine identical cells, similar in construction to the single cell tested. Each cell would contain either microsphere insulation or a reference insulation. The contents of the nine cells are listed below:

- Cell #1 - Uncoated microspheres with aluminized boundaries
- Cell #2 - Uncoated microspheres with black boundaries

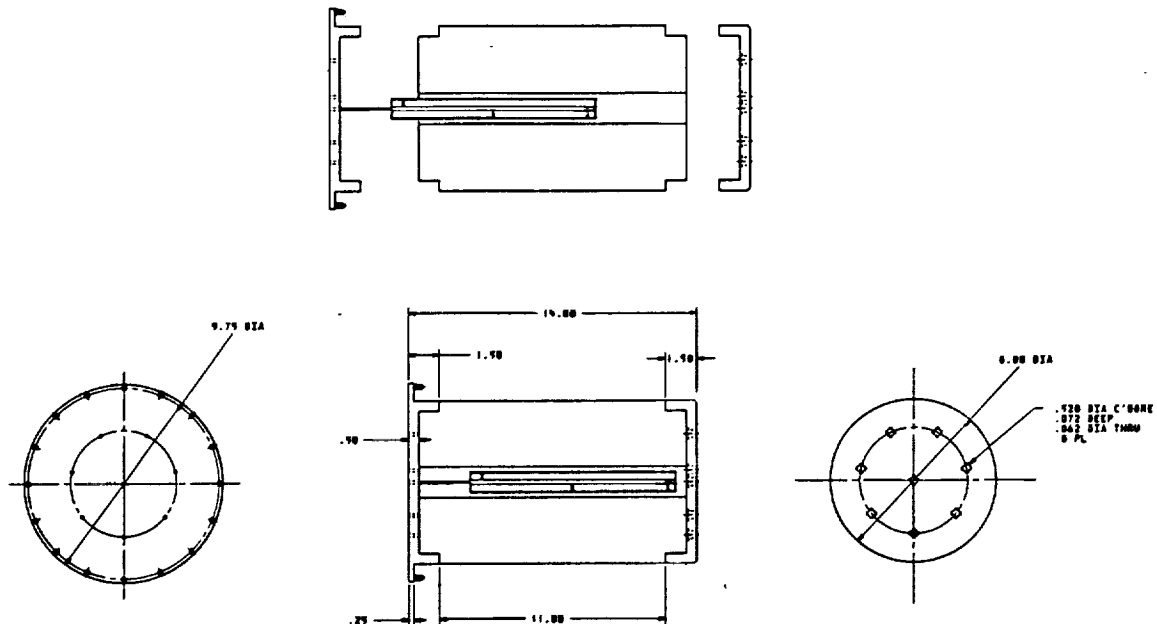


Fig. 3-38 Microsphere Flight Experiment

- Cell #3 - metallized microspheres with aluminized boundaries
- Cell #4 - metallized microspheres with black boundaries
- Cell #5 - metallized and uncoated with aluminized boundaries (50/50 mix)
- Cell #6 - metallized and uncoated with black boundaries (50/50 mix)
- Cell #7 - Radiation with aluminized boundaries
- Cell #8 - Radiation with black boundaries
- Cell #9 - MLI (double aluminized mylar/3 silk net spacers, ~ 9 layers total)

The insulation tests identified will help characterize microsphere performance by bracketing the effect of boundary emissivity from a very low-emissivity surface ( $\epsilon < 0.03$ ) to a relatively high-emissivity surface ( $\epsilon > 0.9$ ). Further, a comparison between uncoated and coated (metallized) can be made for both ranges. Previous ground tests indicate that a combination of coated and uncoated microspheres offers the best thermal protection when conduction is present. Two cells with this mixture would allow comparison in a 0-g environment to the two previous microsphere insulations. The final three cells would test the references for comparison. They include radiation only surfaces to bracket the results and a standard MLI blanket which is currently used on flight cryogenic systems.

### 3.5.2 Microsphere Test Internal Electronics

Each test cell will use calibrated silicon diodes to measure the temperature of the cavity and the hot boundary of the insulation test space. Each diode will use four 5-mil manganin wires for maximum accuracy. A calibrated germanium temperature sensor will be used on the main aluminum block to monitor its temperature. A backup sensor will also be provided. The experiment should operate near 2 K, since it mounts directly to the SFHe tank. Three Minco thermofoil heaters (HK-5263-R280-L12-A) are used to apply heat to the insulation test space. They are connected in series to have a combined resistance of 840  $\Omega$ . The heaters will be bonded down the length of the hot-boundary tube 120° apart. The temperature of the cavity is controlled to be equal to the hot boundary temperature by two Minco heaters (HK-5261-R135-112-A) in series. The heaters will have a combined resistance of 270  $\Omega$ . The heaters will be bonded around the circumference of the central isothermal cavity tube, above and below the spoke standoff.

The heaters were sized to provide power levels from 0.1 mW to 2 W on 0.5 to 28 VDC. These results are shown in Fig. 3-39. The lower power levels are required for insulation performance measurements, while the higher levels provide faster temperature changes and reduce the time to reach steady-state conditions. As shown in Fig. 3-39, these heaters will limit the current to less than 0.2 A, which allows the use of 10-mil manganin wire in a vacuum.

### 3.5.3 Low-g Performance of PODS

During the integration phase of this experiment, the dynamic characteristics of the PODS will be analyzed to determine the location of the accelerometers required to investigate the low-g performance of the PODS. The results of this experiment will help to determine whether coupling between the liquid-helium sloshing and the inherent low frequency of PODS in orbit is a serious concern. Two sets of x, y, and z accelerometers will be used for redundancy on the SFHe tank, and a third set will be mounted in the electronics package outside of the HELD as a reference.

## 3.6 INTEGRATION OF FLIGHT EXPERIMENT WITH HELD

### 3.6.1 Integration With HELD

The experimental package is designed to be mounted inside the superfluid tank of HELD. The integrated package is shown in Fig. 3-40. The design of HELD, shown in Fig. 3-41,

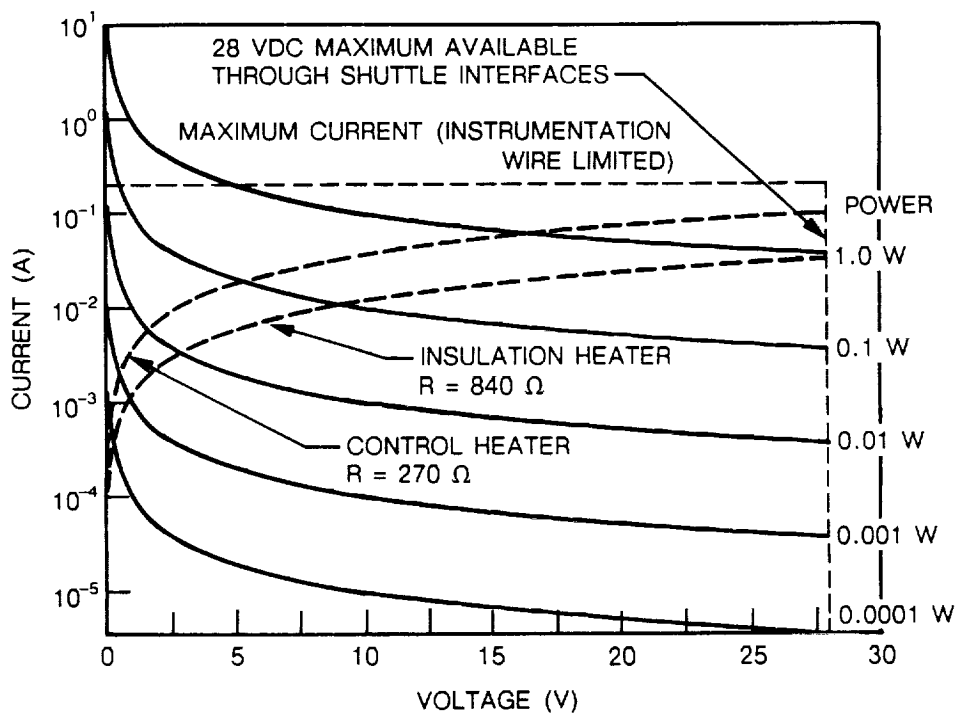


Fig. 3-39 Power Requirements for Microsphere Heaters

permits the package to be mounted and dismounted by removing the top vapor-cooled shields and folding back the insulation. The experiment package will share a common vacuum with HELD by using  $20\text{-}\mu\text{m}$  porous plugs in the bottom of each cell. The instrumentation wires come out of the top of the experiment and can be routed down the PODS to minimize parasitic heat loads. Hermetically sealed connections in the vacuum shell mounting ring of the HELD provide interfacing with ground support systems and with the flight electronics.

### 3.6.2 Integration with IFPA

Another experiment chosen for the outreach program deals with an Infrared Focal Plane Assembly (IFPA) developed at LMSC that must be cooled down below  $8\text{ K}$ . One advantage of using the HELD dewar is that multiple experiments can be integrated together into a larger experiment package that would only require one flight. This particular package could attach to the bottom of the microsphere cold-boundary well with no adverse affect to either experiment. The proposed combined package is shown in

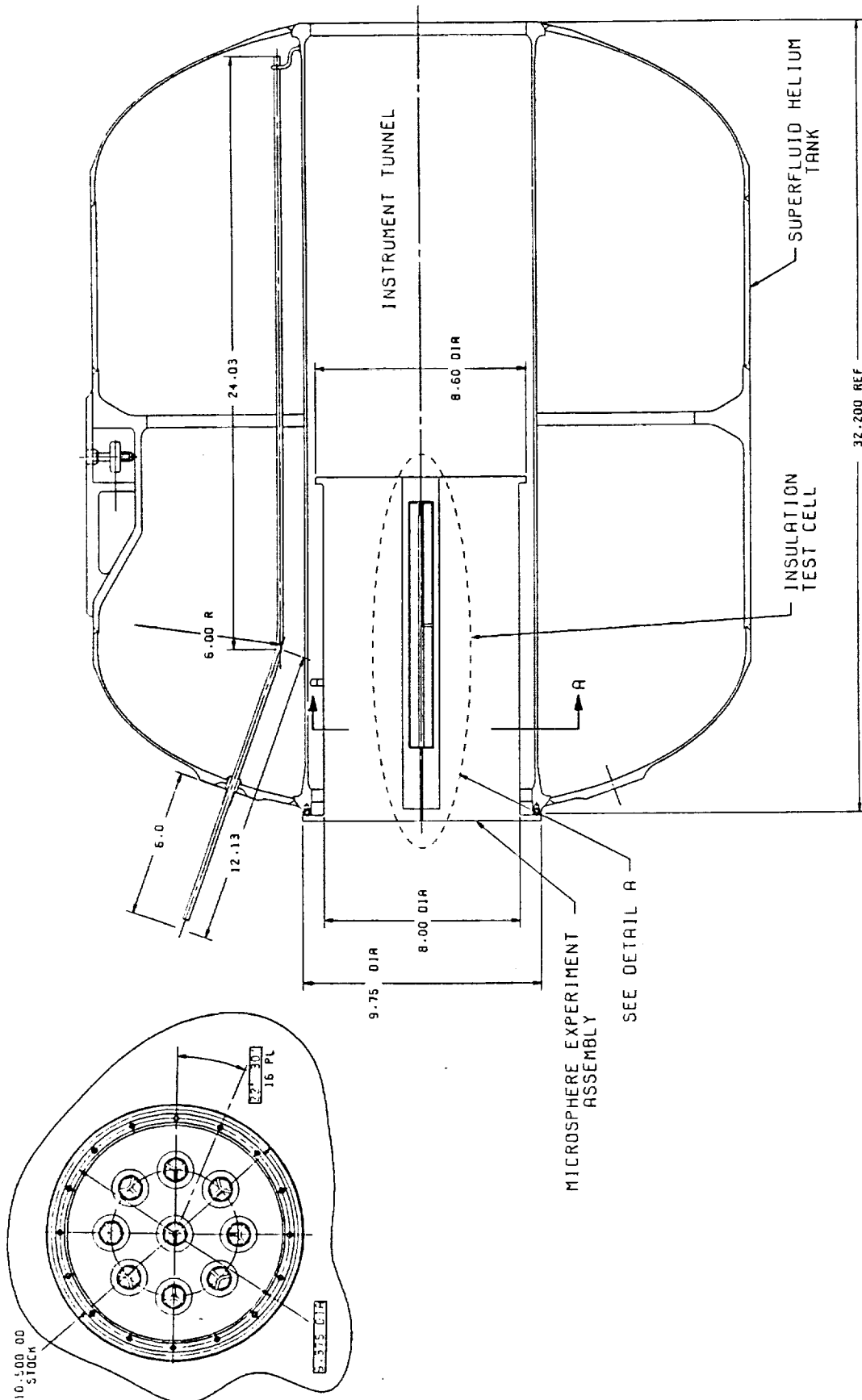


Fig. 3-40 Integration of Experiment Into HELD

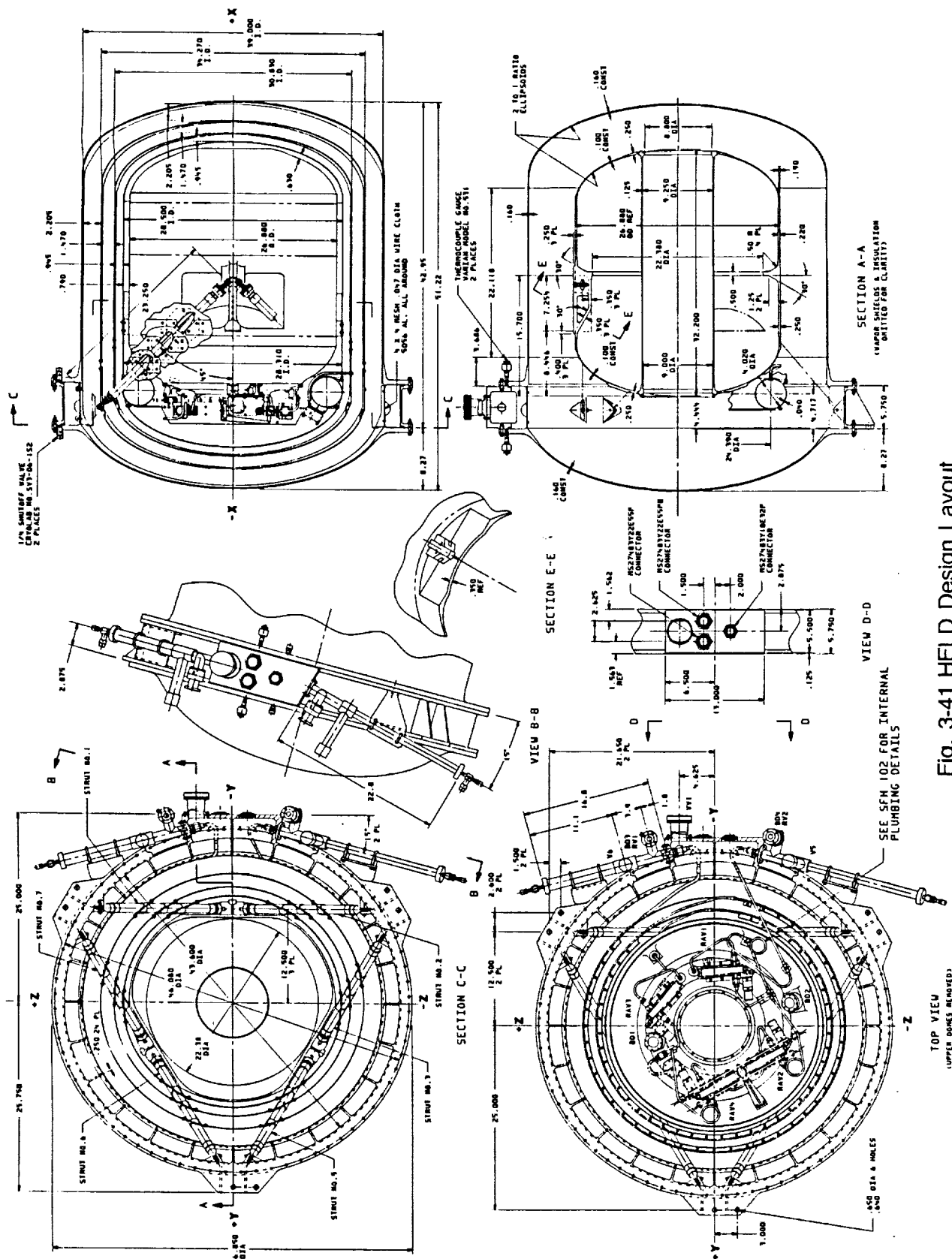


Fig. 3-41 HELD Design Layout

Fig. 3-42. Cabling for the IFPA can be routed out the top through the vapor-cooled shields, similar to the microsphere instrument wiring.

### 3.6.3 Lifetime

HELD was designed to provide 9 months of helium lifetime with an experiment heat load of 15 mW to the SFHe tank and a 300-K vacuum shell. The microsphere test cells are predicted to produce between 200 and 300 mW of steady-state heat input into the SFHe tank when the experiment is turned on. The predicted lifetime of the dewar with this experiment is shown in Fig. 3-43. HELD is currently undergoing thermal testing to verify this prediction.

### 3.6.4 Ground Hold

One advantage of HELD is that it offers simplified prelaunch servicing by having a normal boiling point (NBP) helium guard tank on the first vapor-cooled shield. The purpose of this guard tank is that it allows the SFHe tank to be filled and valved off prior to launch. The NBP tank is then filled and provides a 4.2-K guard shield around the SFHe tank, resulting in extremely low heat rates to the SFHe. This allows the SFHe to remain in an unvented condition for an extended period as long as the guard tank is maintained at 4.2 K. The NBP tank is allowed to vent during ground hold and can repeatedly be refilled as needed prior to launch.

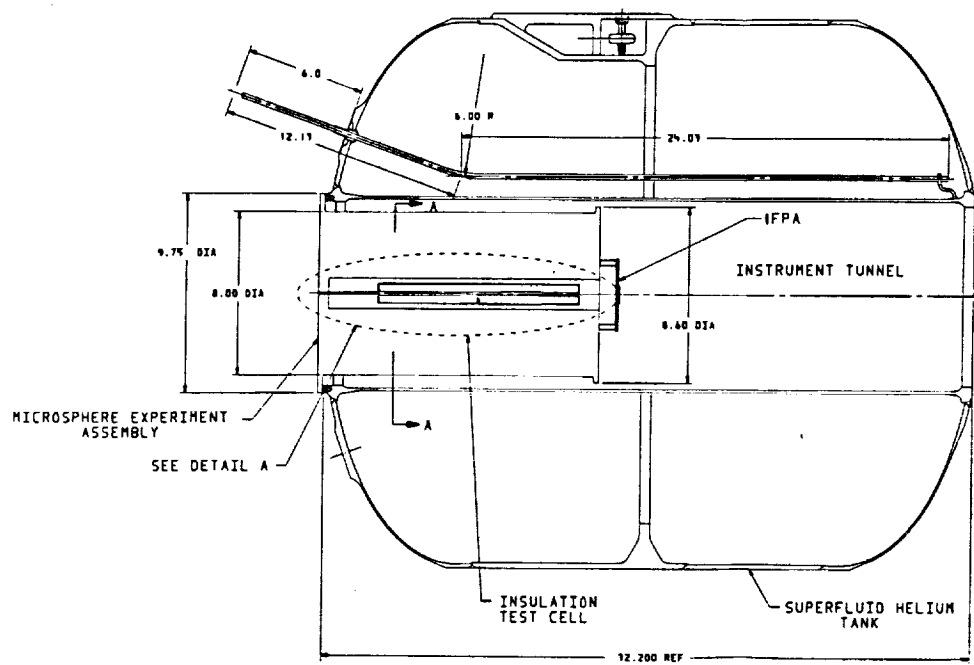


Fig. 3-42 IFPA/Microsphere Assembly

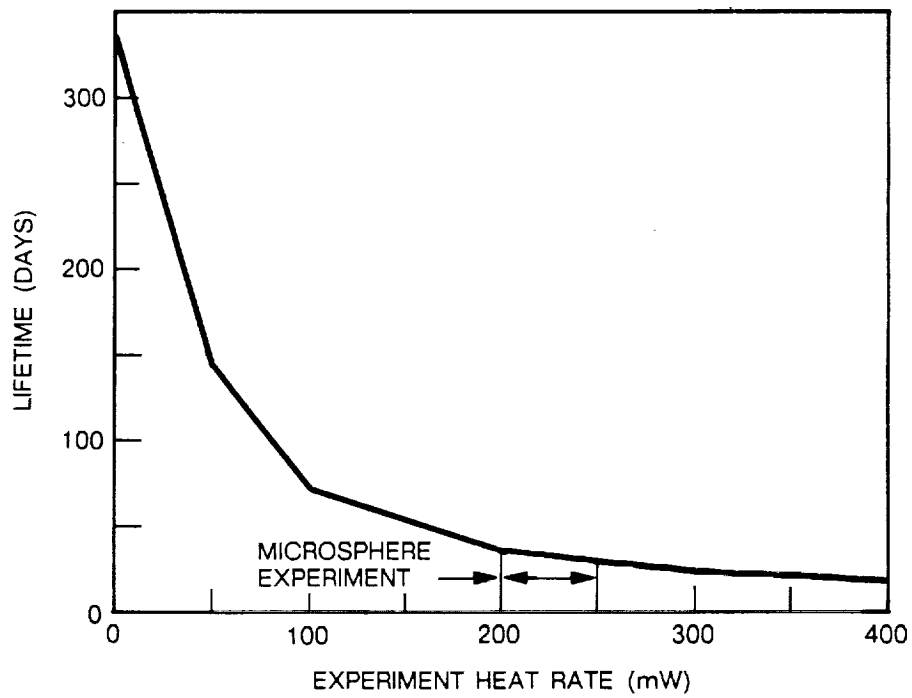


Fig. 3-43 Effect of Experiment Heat Rate on HELD Lifetime

## Section 4

### INTEGRATION WITH HOST SPACECRAFT

#### 4.1 HITCHHIKER M

##### 4.1.1 Mechanical Interface

The HELD and accompanying flight electronics will be mounted on one of the new extension capabilities of the Space Transport System (STS), the HITCHHIKER-M (HH-M) (Fig. 4-1). The HH-M, developed by Marshall Space Flight Center (MSFC), is a standardized mechanical platform which will carry up to 1200 lb of equipment mounted on a cross bay bridge structure in the Space Shuttle. The HH-M will also be equipped with an avionics control unit that gives the customer easy access to the orbiter resources from which a total system can be configured.

Figures 4-2 and 4-3 show HELD installed on the HH-M. The dewar will occupy the top of two bays of the HH-M. The two HH-M bays can accommodate 760 lb for this configuration. Table 4-1 lists the HELD component weights for the system. The flight electronics box is not shown but will mount to the front of the HH-M, which can support 170 lb.

##### 4.1.2 Plumbing Interface

The SFHe tank must be able to be serviced after integration with the HH-M by refilling the NBP helium guard tank with liquid helium in order to prevent the SFHe from reaching the lambda point before launch. Figure 4-4 shows the plumbing schematic. Both tanks are loaded through a single fill line (V5-RAV1 for the SFHe tank and V5-RAV2 for the normal helium tank) and vented through a common vent line (RAV3-RAV4-V6 during loading or RAV4-V6 in orbit for the SFHe tank, and V6 for the guard tank). The SFHe tank is filled and conditioned first and then valved off. The guard tank is filled and allowed to vent during ground hold, launch, and orbit until it is empty. RAV4 is then opened so the SFHe tank vents through the porous plug for the remainder of the mission.

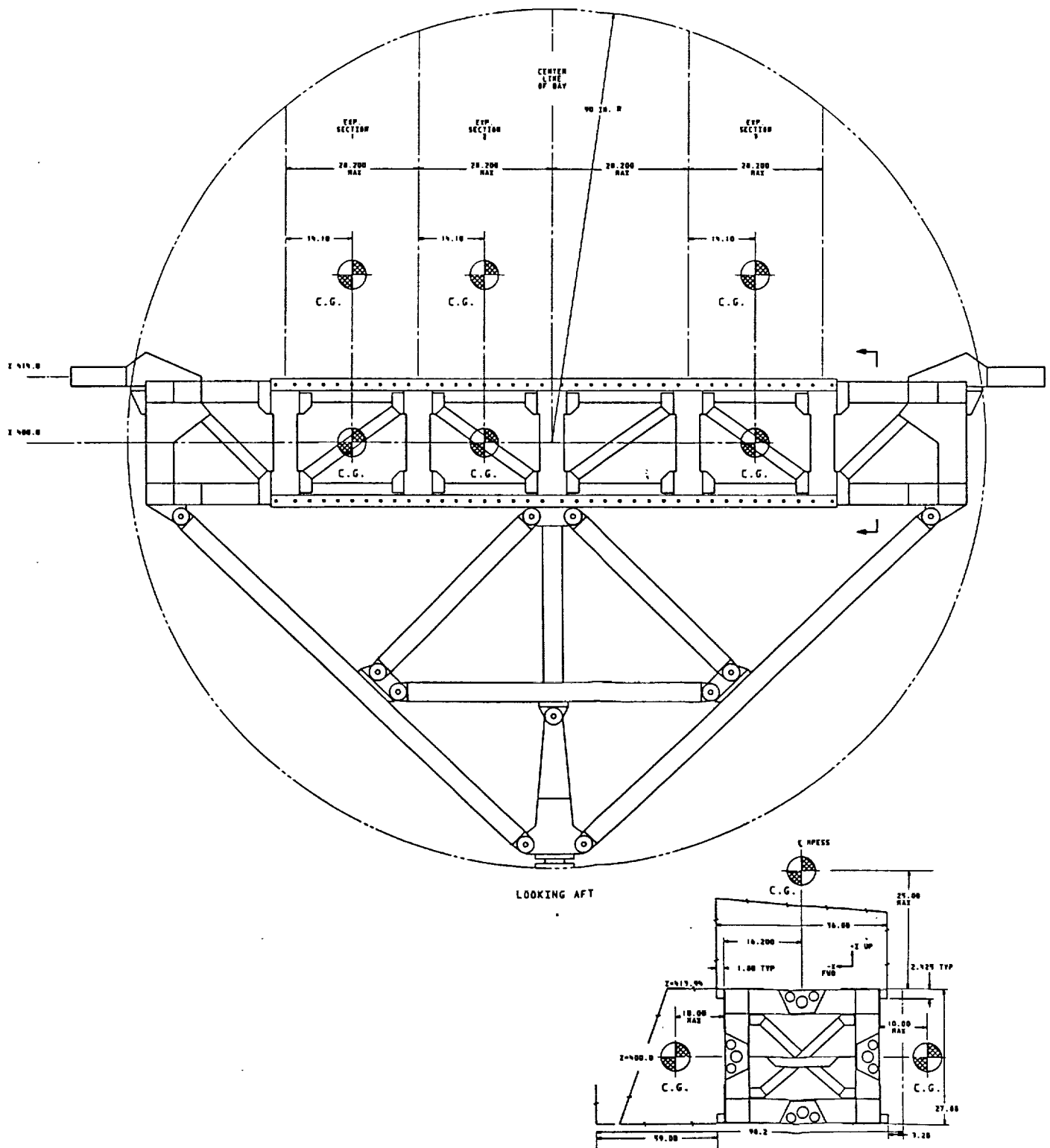


Fig. 4-1 HH-M



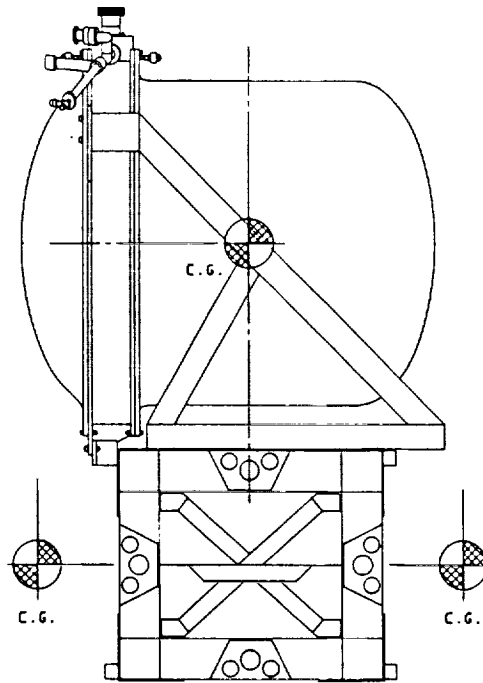


Fig. 4-3 HELD-HHM Integration (Side View)

Table 4-1 WEIGHT SUMMARY (lb)

He-II Tank and Plumbing	106
200-L He-II	55
He-I Tank	9
15-L He-I	2
Vapor-Cooled Shields (3)	66
MLI	25
PODS (6)	8
Support Ring	52
Vacuum Ring	102
External Plumbing	5
Miscellaneous	<u>10</u>
Total HELD Launch Weight	440
Experiment Package	25
Flight Electronics	30
HH-M Interface Support Structure	<u>50</u>
Total Launch Weight	545

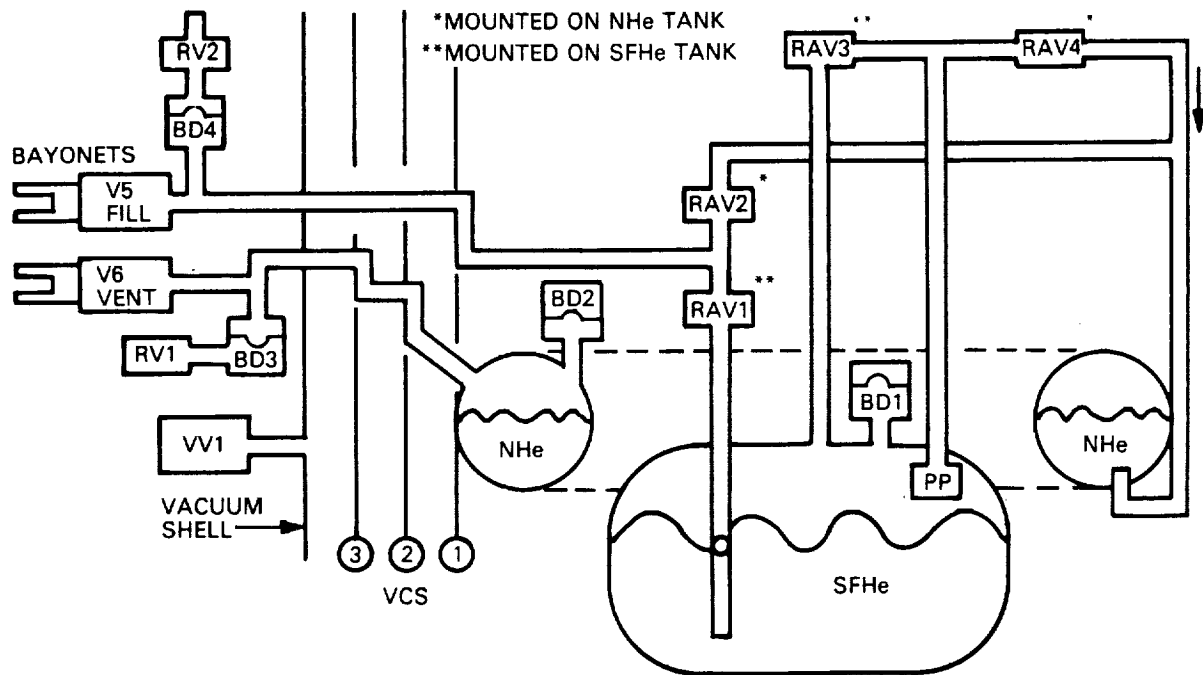


Fig. 4-4 Fluid System

#### 4.1.3 Electrical/Data Interface

The HH-M is equipped with an avionics control unit that enables easy access to the orbiter resources, from which a total system can be configured, as shown in Fig. 4-5. Command sequences and data transfers will follow the system path as shown. The microsphere experiment payload will first be powered by a command from the ground to orbiter communication uplink. The payload experiment will then collect data approximately every 15 min and transfer data to the HH-M avionics unit. The data will then be translated and transferred to the customer carrier ground support equipment, which translates these data and sends the data to either the low rate ground support equipment (LRGSE) or the customer ground support equipment (CGSE). Both of these devices will record the data for future data reduction. After the experiment is complete, the mission command center will send the command to power down the payload through the uplink. The LRGSE provides the means to record the payload data as well as any required ancillary data (e.g., payload temperature, bus voltage, relay states). Further descriptions of communications can be found in Refs. 10 and 11.

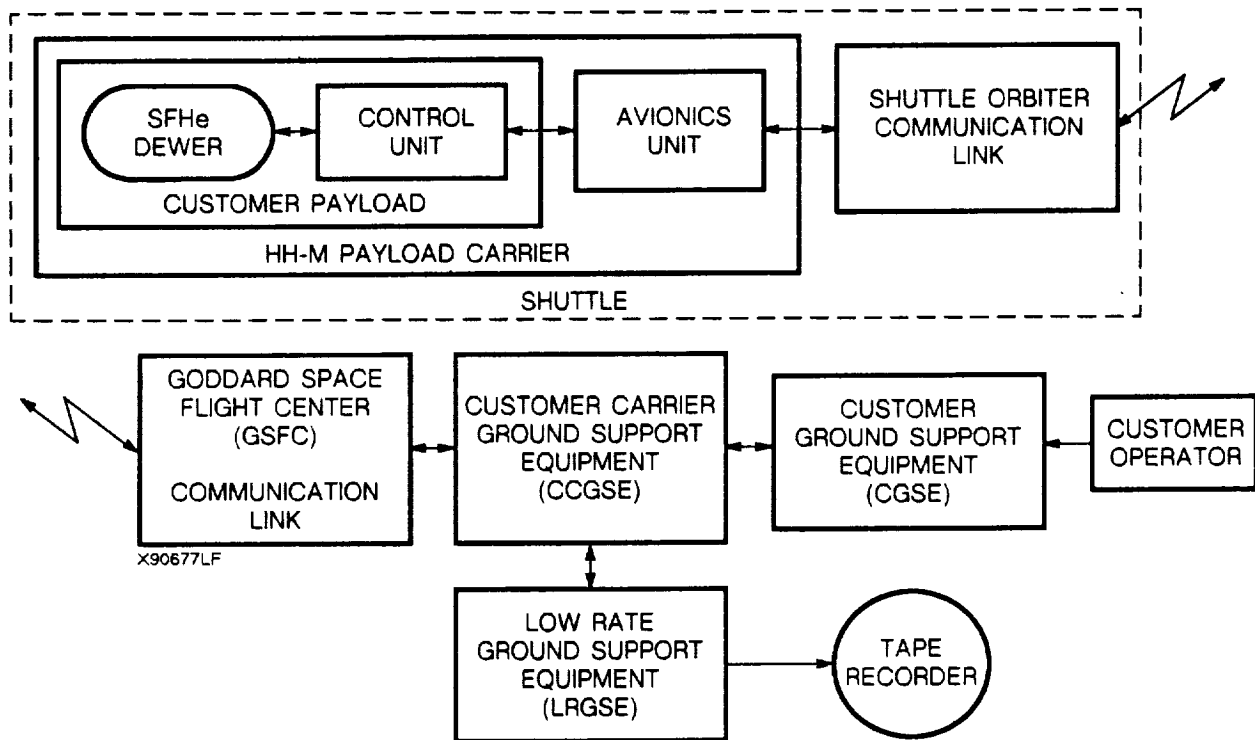


Fig. 4-5 ICE Microsphere Payload System Configuration

#### 4.1.4 Customer Ground Support Equipment

The CGSE unit will essentially be a small portable IBM-AT compatible computer configured with a communication box to simulate the orbiter avionics control signals. This communication box is required to maintain the interface standard provided by the transparent data and command system concept set by the HH-M system.

The computer will be a Compac portable 286 style III, running at 20 MHz with a RS-232 communication link, a parallel port, a 40-Meg hard disk, and a 1.2-Meg/360-K floppy disk.

The communication box is a simple signal converter box which will receive the RS-232 and parallel signal information from the Compac computer. The box will convert these signals to compatible CGSE control signals, which are the same as the interface signals from the orbiter avionics unit to the experiment payload control unit. The component's power and size requirements are:

- Power requirements
  - Compac 286: 120 AC @ 200 mA
  - Communications box: 120 AC @ 50 mA
- Mechanical space requirements
  - Compac 286: 18 in. wide × 10 in. high × 10 in. deep
  - Communications box: 10 in. wide × 4 in. high × 7 in. deep

#### 4.1.5 Measurement Electronics Payload

The electronics payload will consist of two major elements, the control unit and the SFHe dewar. The control unit will supply all the necessary interfaces from/to the orbiter avionics unit and to/from the SFHe dewar, as shown in Fig. 4-6.

The avionics/control unit interface primarily passes collected experimental data to the ground data tape recorders but also has the capability to reset the processor, monitor payload temperatures, and connect/disconnect primary power. The avionics unit interface

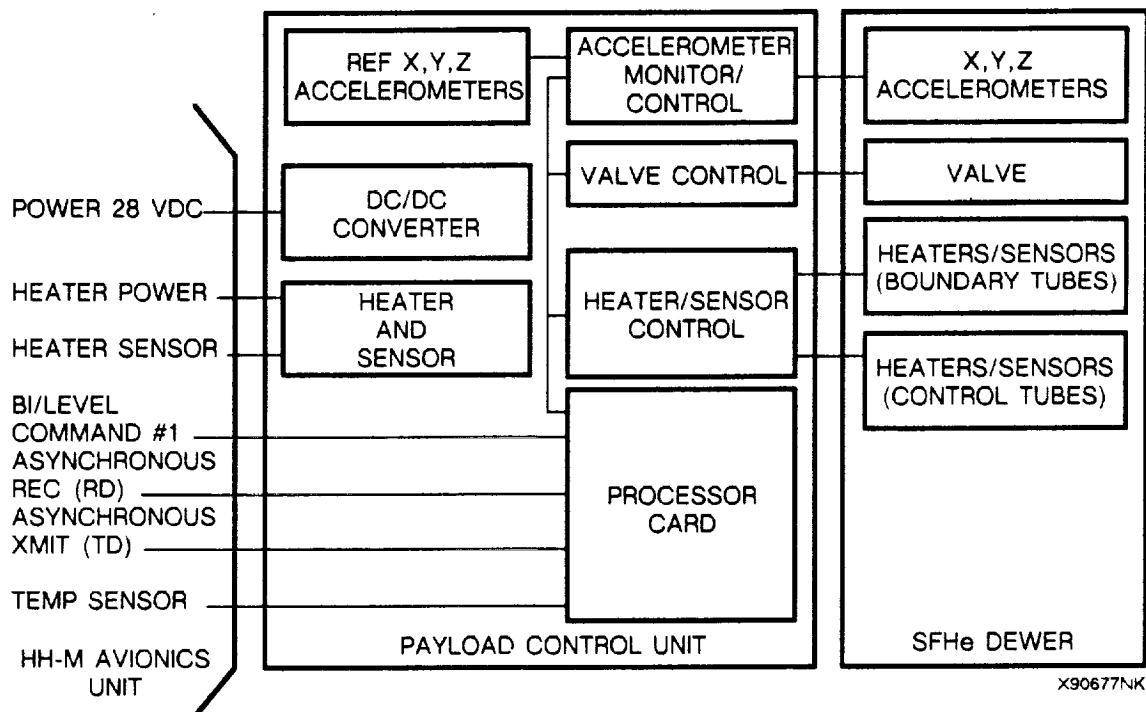


Fig. 4-6 ICE Microsphere Measurement System Block Diagram

also contains temperature and heater control signals to regulate the control unit's temperature between -20°C to +60°C when primary power is off or on.

The control unit/SFHe dewar interface signals consist of heater power for 18 heating elements, 20 temperature sensors, 5 helium valve controls and limit switches, and 2 accelerometers.

The control unit controls all aspects of the experiment when primary power is applied. The control unit processor's primary objective is to control/monitor heater temperature and monitor acceleration forces and save these data in complete redundancy with the onboard Eprom and the ground-based tape recorder at GSFC. The control unit consists of eight control cards; the processor card, five heater control/monitor cards, a valve control card, and an accelerometer control/monitor card. The power and size requirements for the system are:

- Power requirements
  - Payload: 162 W @ 28 VDC
- Mechanical space requirements
  - Control Unit: 15 in. wide × 10 in. high × 10 in. deep

## **4.2 SAFETY**

The philosophy and approach to safety for HELD are similar to that of the Superfluid Helium On Orbit Transfer (SHOOT) flight demonstration, in that all potential hazards will be controlled through passive mechanical devices such as burst discs or relief valves, and no electronic or operator commands will be required to initiate a hazard control at any time.

### **4.2.1 HELD Dewar Structural Analysis**

The SFHe tank of HELD is supported at its effective center of gravity by six PODS struts which contain a pair of concentric tubes: an outer launch tube and an inner orbit tube. During launch, the inner tube elastically elongates or compresses until the launch tube is engaged. In this condition, the PODS are said to have "shorted," since the thermal disconnect gap has been negated. Once the system is in orbit and the launch loads have been removed, the orbit tube resumes its original position, reestablishing the thermal gap and resulting in increased thermal resistance. These struts were developed and structur-

ally tested under previous NASA contracts. Further information on their structural and thermal performance can be found in Refs. 6, 7, 8, and 9.

HELD is currently undergoing structural evaluation and has undergone extensive structural analysis. The SFHe tank, support struts (PODS), torus NBP tank, and torus support skirt have been modeled on NASTRAN and subjected to longitudinal and lateral 20-g launch loads and frequency calculations. The first two launch frequencies are 43.9 and 44.2 Hz, reflecting a rocking motion in the horizontal plane, with the top of the tank vessel doing most of the moving, i.e., when the top moves horizontally one unit of displacement, the bottom moves about one tenth as much and in the opposite direction. The first axial mode is at 72.2 Hz. Except for the struts, the stresses in the vessel are very low for both the axial and lateral 20-g loads. For the axial 20-g load, the struts are loaded at approximately 40% of their elastic buckling failure strength. For the lateral 20-g load, the highest loaded strut sees 77% of elastic buckling failure strength.

The SFHe tank, NPB tank, and vacuum shell have been designed as pressure vessels, capable of withstanding the pressure obtained prior to burst disc or relief valve operation with the required safety factor of 4. The SFHe tank is capable of withstanding a burst pressure of 116 psi and collapsing pressure of 30 psi (1 atm, with a factor of safety of 2). The NBP tank also is capable of withstanding a burst pressure of 116 psi and a collapsing pressure of 30 psi. The vacuum shell is capable of withstanding a burst pressure of 24 psi and a collapsing pressure of 45 psi. BOSOR4 and PANDA codes were used to evaluate this design.

#### **4.2.2 HELD Catastrophic Vent Analysis**

Catastrophic loss of vacuum, i.e., puncture of the vacuum shell, allows air to solidify on the tanks, driving the tank heat rates extremely high. Due to the resulting large vent rates, it is not possible to vent the helium out of the normal fill or vent lines rapidly enough to prevent bursting of the tanks. Consequently, the emergency relief system selected dumps the helium directly into the vacuum cavity through burst discs BD-1 and BD-2 (Fig. 4-7). The helium vents out of the vacuum shell through VV1 and the damage hole in the shell. A coarse screen located on the inside circumference of the vacuum support ring prevents potential debris, i.e., torn MLI, from clogging VV1.

The program HELM 75 was used to calculate the pressure response in the tanks. This program has been verified against actual test data using a copper tank calorimeter filled

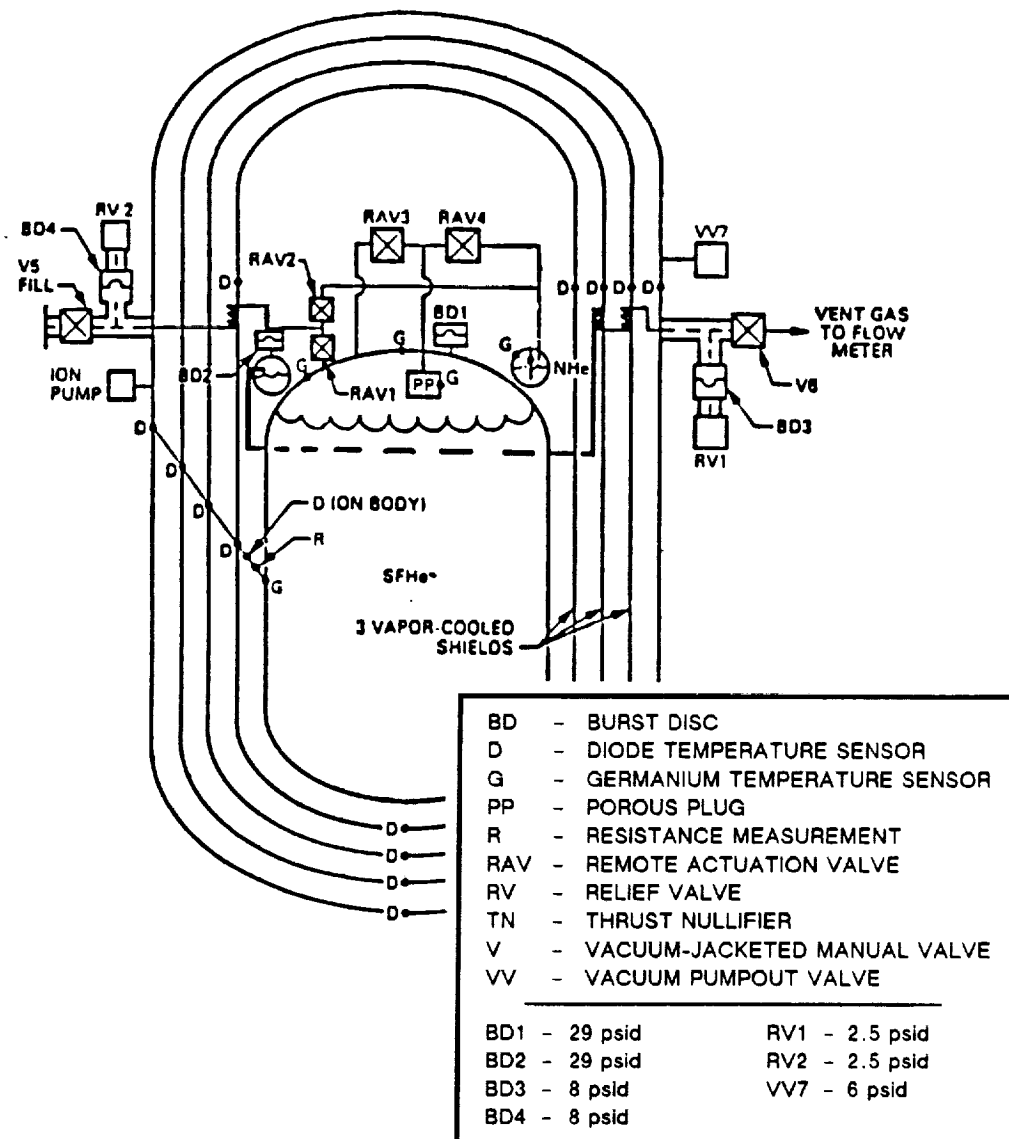


Fig. 4-7 HELD Plumbing Diagram

with normal helium, with and without MLI installed on the tank. A gate valve provided the sudden loss of vacuum and tank exposure to 1-atm pressure. Figure 4-8 (SFHe tank) and Fig. 4-9 (normal helium) present the calculated tank pressure responses. The liquid helium fraction (LHF) in the tank is assumed to be 48.7%, such that only supercritical helium is discharged into the space between the outer shell. Previous analyses show that lower values of liquid helium yield lower values of maximum dewar pressure after rupture of the burst disc.

	DISC SIZE (cm)	$P_{max}$ (MPa)	$t_{max}$ (s)	$t_e$ (s)	$T_e$ (K)
A	1.17	0.3598	8	136	63.6
B	1.27	0.3439	6	121	60.5
C	1.59	0.3119	3	90	51.3 (SELECTED)
D	1.91	0.3012	0	73	44.3

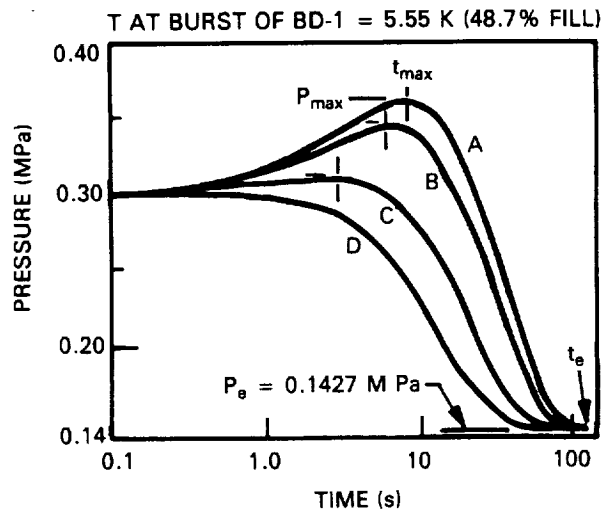


Fig. 4-8 SFHe Tank Pressure After Burst of BD-1

	DISC SIZE (cm)	$P_{max}$ (MPa)	$t_{max}$ (s)	$t_e$ (s)	$T_e$ (K)
A	1.17	0.3101	0.3	12.2	53.46
B	1.27	0.3034	0.2	10.8	48.85
C	1.59	0.3012	0	8.1	38.3 (SELECTED)
D	1.91	0.3012	0	6.3	29.5

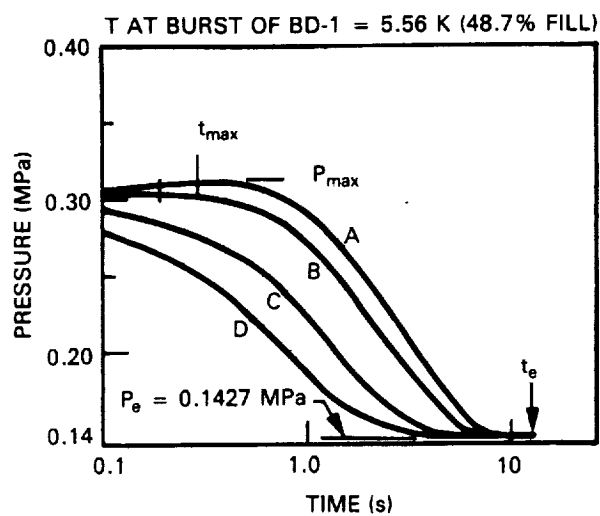


Fig. 4-9 SFHe Tank Pressure After Burst of BD-2

## Section 5

### APPLICATIONS

The potential applications for microsphere insulation systems fall into two categories: (1) long-term cryogenic storage with low hot boundary temperatures, and (2) propulsion systems that utilize a foam insulation with a helium purge. Only microsphere applications in long-term cryogenic storage were investigated in this study.

Since microsphere performance is potentially comparable to that of MLI for hot-boundary temperatures less than 100 K, microspheres would only be considered for long-term cryogenic storage applications with low hot-boundary temperatures. Two proposed experiments that meet this criteria are the Space Infrared Telescope Facility (SIRTF) and the X-Ray Spectrometer (XRS).

SIRTF is considering a very high-altitude orbit to cool the vacuum shell and extend cryogen lifetime. A preliminary study of this orbit indicates an average shell temperature of 100 K. This low boundary temperature makes SIRTF a candidate for microsphere insulation. XRS is a SFHe-cooled experiment that will fly on the Advanced X-Ray Astronomical Facility (AXAF). XRS does not have a cold vacuum shell (244 K), but it does utilize mechanical refrigerators to cool the outer vapor-cooled shield (OVCS) to 70 K. For XRS, it would only be practical to use microspheres inside the OVCS and MLI between the OVCS and the vacuum shell.

Table 5-1 compares the cryogen lifetime of these two experiments for standard MLI systems and microsphere systems. In both applications, the uncoated microspheres do not perform as well as the MLI, but the aluminized microspheres increase the lifetime by 20%. The greater decrease in life for SIRTF using uncoated microspheres is due to the warmer boundary temperature (100 K versus 70 K).

These results indicate that microspheres have the potential to perform as well or better than MLI. If the installation is less costly, then microspheres could compete with MLI for

Table 5-1 LONG-TERM CRYOGEN STORAGE  
APPLICATIONS FOR MICROSPHERES

Insulation System	Cryogenic Experiment Lifetime (years)	
	SIRTF	XRS
MLI	7.0	6.0
Uncoated Microspheres	4.0	5.6
Metalized Microspheres	8.8	7.2

certain applications. It should be noted that the two experiments studied were optimized for MLI, not microspheres. Optimizing them for microsphere insulation may change the vapor-cooled shield locations and improve the system performance.

## Section 6

### PRELIMINARY COST ESTIMATE

The preliminary cost estimate is for the design, fabrication, testing, and data reductions required for the microsphere experiment proposed. The cost estimate is provided in a separate document, LMSC-F362496. The costing is based on the Work Breakdown Structure (WBS), program schedule, and test flow, presented in Figs. 6-1, 6-2, and 6-3. The second-level WBS elements are as follows:

- 1.1 Management—The program controls on cost and schedule, configuration management, administration, and technical publications
- 1.2 Product Assurance—Safety, reliability, quality assurance engineering, and inspection
- 1.3 Engineering & Design—All of the analysis necessary to complete the design of the experiment, electronics, and experiment integration
- 1.4 Manufacturing—All of the labor and materials necessary to fabricate and assemble the flight experiment
- 1.5 Test—Testing, data reduction, and documentation of subsystem, system, and flight tests
- 1.6 Ground Support Equipment—Design, fabrication, and assembly of all fixtures, handling equipment, service equipment, and containers necessary for the experiment
- 1.7 Payload Integration—This is primarily the labor necessary to support the integration of the experiment with HH-M and the Shuttle

The program schedule (Fig. 6-2), shows 30 months from the program start date to the launch. The test flow in Fig. 6-3 shows subsystem and system tests. At the subsystem level, the experiment package would go through liquid nitrogen and NBP helium tests to

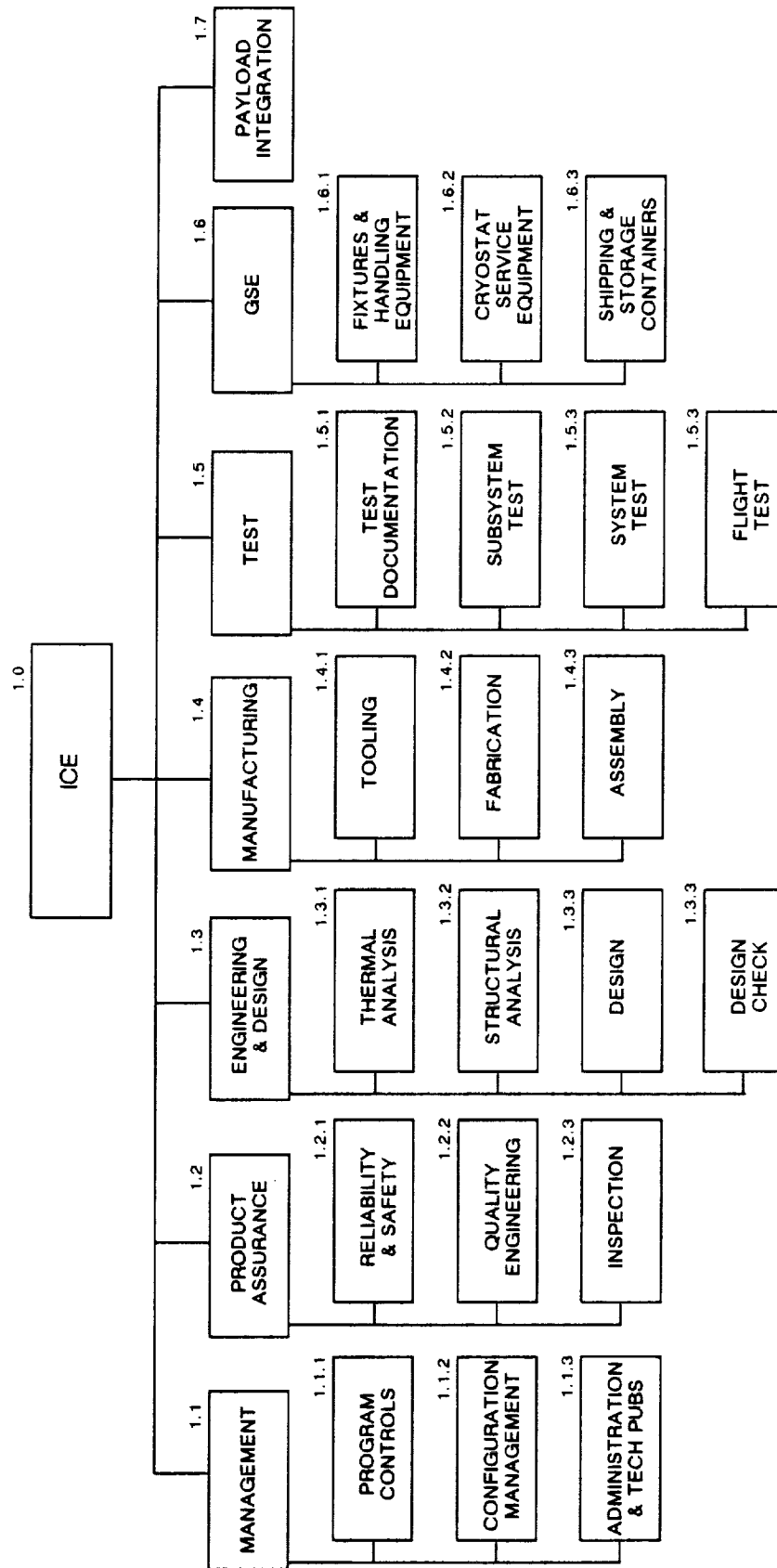
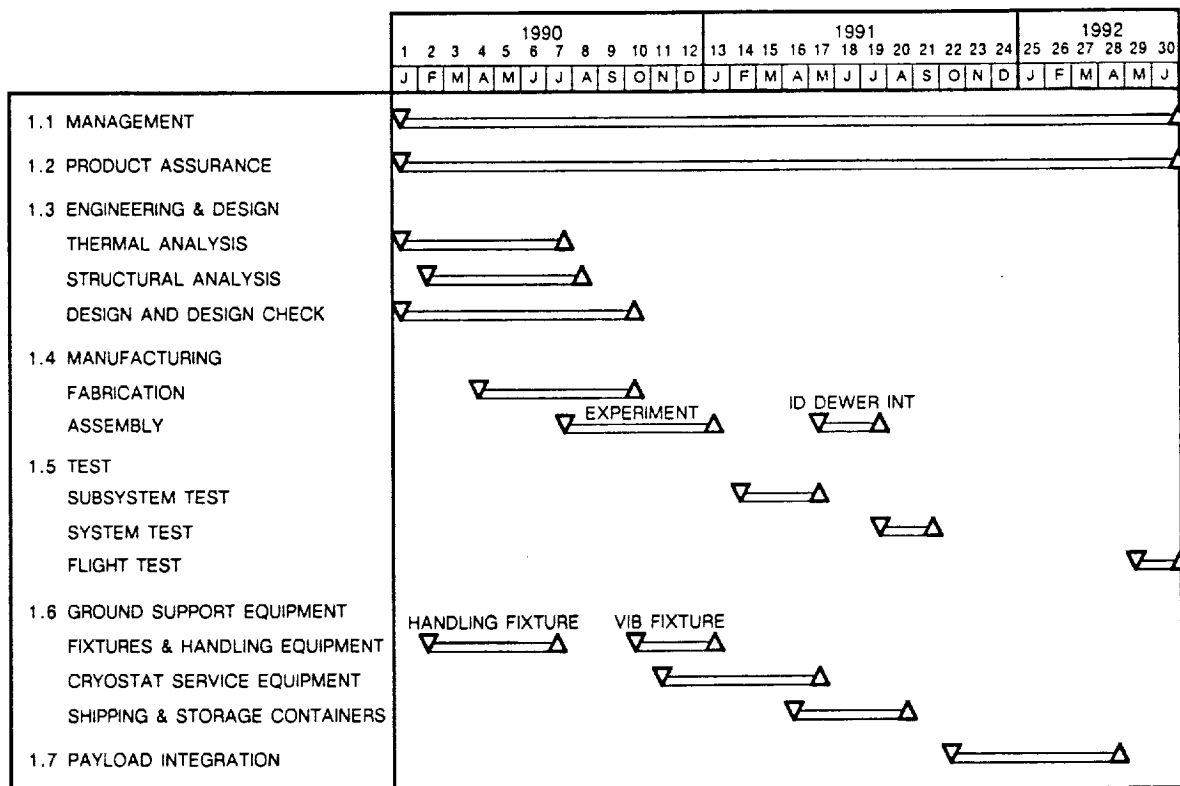


Fig. 6-1 Microsphere WBS



X90677LF

Fig. 6-2 Microsphere Program Schedule

characterize the experiment performance. The experiment package would then be subjected to the appropriate environmental testing and retested with helium before being integrated with HELD for system testing.

The flight electronics would undergo the appropriate functional tests before and after environmental and thermal vacuum testing. The electronics would then be incorporated for systems testing. HELD does not have any subsystem tests, since it will have been previously qualified by LMSC.

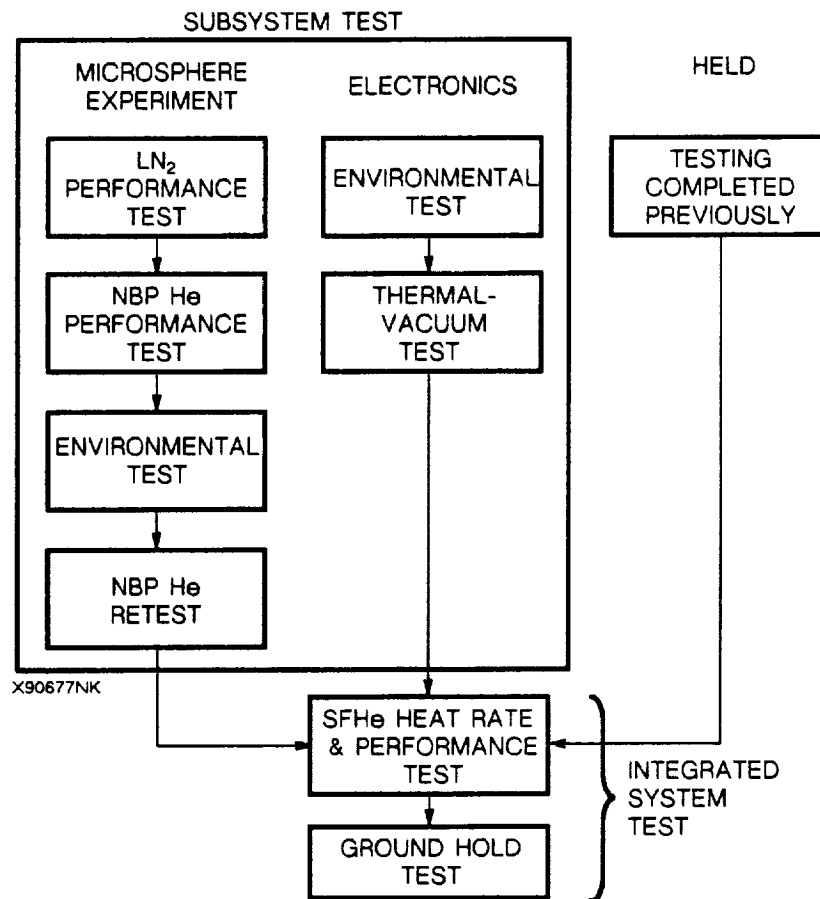


Fig. 6-3 Test Flow

## Section 7

### SUMMARY AND CONCLUSIONS

The analysis presented in this report indicates that microsphere insulation has the potential to be useful for cryogenic systems. In addition to its performance potential, its isotropic nature makes its performance more repeatable and less susceptible to variation caused by different installation techniques. The installation of microspheres would be less labor intensive than current MLI systems, which would result in less expensive cryogenic systems with minimal reduction in thermal performance.

The major conclusions from this study are:

- Microspheres have the potential to be a useful insulation for particular applications, including vacuum systems with boundary temperatures less than 100 K (e.g., SIRTf, XRS) and possibly in gas purged systems.
- A flight experiment to determine microsphere behavior and performance is required due to the significant predicted improvement in thermal performance in 0 g.
- The proposed experiment evaluates the most critical parameters such as boundary emissivity and surface coating to improve the understanding and predictions of microsphere performance.
- Ground testing has validated the proposed experiment configuration and control technique.
- The experiment can be installed in HELD which is currently undergoing extensive thermal and structural testing. HELD's design permits integration with other experiments requiring SFHe cooling, resulting in a larger package that would require only one flight.
- The use of HELD for the test bed permits low-g dynamic characterization of PODS to determine the interaction with the sloshing liquid helium. HELD also demonstrates other technologies that have been incorporated into its design

such as improved MLI, low-conductance fill line, porous-plug vent, PODS-supported vapor-cooled shields, and simplified prelaunch servicing due to a NBP guard tank.

Demonstration of these technologies will benefit NASA cryogenic programs such as: SIRTf, AXAF, Gravity Probe-B, Astromg, Superfluid Helium Tanker, and COLD-SAT.

## Section 8

### REFERENCES

1. Lockheed Missiles & Space Company, Inc., *Evacuated Load-Bearing High Performance Insulation Study*, NAS3-17817, NASA-CR 135342, Dec 1977
2. G. R. Cunningham and C. L. Tien, "Heat Transfer in Microsphere Cryogenic Insulation," *Advances in Cryogenic Engineering*, Vol. 18, Plenum Press, New York, 1973, p. 103
3. R. T. Parmley and G. R. Cunningham, "An Ultra-Lightweight, Evacuated, Load Bearing, High Performance Insulation System," 2nd AIAA/ASME Thermophysics and Heat Transfer Conference, May 1978
4. M. G. Kaganer, *Thermal Insulation in Cryogenic Engineering*, Isreal Program for Scientific Translations, Jerusalem, 1969
5. G. R. Cunningham, C. W. Keller, and G. A. Bell, *Thermal Performance of Multilayer Insulation*, NASA-CR 72605, Apr 1971
6. R. T. Parmley, *Passive Orbital Disconnect Strut (PODS-III) Structural and Thermal Test Program*, NASA CR 166473, Mar 1983
7. R. T. Parmley, *Passive Orbital Disconnect Strut (PODS-III) Structural Test Program*, NASA CR 177325, Jan 1985
8. R. T. Parmley, *Test and Evaluate Passive Orbital Disconnect Struts (PODS-III)*, NASA CR 177368, Aug 1985
9. I. Spradley, *Passive Orbital Disconnect Strut (PODS-IV) Development*, NASA CR 177426, Sep 1986

10. Marshall Space Flight Center, "Hitchhiker-M/Payload Generic Interfaces," ICD-B-21000-HHM Rev. A, Spacelab Program, Apr 1987
11. Goddard Space Flight Center, "Hitchhiker Shuttle Payload of Opportunity Carrier Customer Accommodations and Requirements Specifications," HHG-730-1503-04, Jul 1988

1. Report No. NASA CR 177538	2. Government Accession No.	3. Recipient's Catalog No.	
4. Title and Subtitle Integrated Cryogenic Experiment (ICE) Microsphere Investigation		5. Report Date September 1989	
		6. Performing Organization Code	
7. Author(s) I. Spradley, D. Read		8. Performing Organization Report No. LMSC-F279204	
9. Performing Organization and Address  Lockheed Missiles & Space Company, Inc. Palo Alto, CA 94304		10. Work Unit No.	
		11. Contract or Grant No. NAS2-12897	
12. Sponsoring Agency Name and Address  National Aeronautics and Space Administration Washington, DC 20546		13. Type of Report and Period Covered Contractor Report	
		14. Sponsoring Agency Code MS 244-10	
15. Supplementary Notes  Point of Contact: Technical Monitors Jeff M. Lee, Ames Research Center, Moffett Field, CA, 94035 (415) 694-3191			
16. Abstract  The microsphere investigation is one of 41 outreach proposals that have been funded for a definition study. The purpose of the investigation is to determine the performance of microsphere insulation in a 0-g environment and compare its performance to reference insulations such as multilayer insulation (MLI). The Lockheed Helium Extended-Life Dewar (HELD) will be used to provide a superfluid-helium (SFHe) cold sink for the experiment. The use of HELD allows the low-g dynamic properties of Passive Orbital Disconnect Struts (PODS) to be characterized and provides a flight demonstration of the PODS system.  This study consisted of predicting the thermal performance of microspheres in 1 g and 0 g, designing a flight experiment to determine microsphere thermal performance, and designing the interface between the experimental package and the shuttle through HELD and the Hitchhiker-M (HH-M) carrier. A single test cell was designed and fabricated. The cell was filled with uncoated glass microspheres and tested with a liquid-nitrogen cold sink. The data were found to agree well with predictions of microsphere performance in 1 g.			
17. Key Words (Suggested by Author(s))  insulation; cryogen storage; analysis design; fabrication; test; outreach		18. Distribution Statement	
19. Security Classif. (of this report) Unclassified	20. Security Classif. (of this paper) Unclassified	21. No. of Pages	22. Price*